Structures 87 (2026) 111742

Contents lists available at ScienceDirect

Structures

journal homepage: www.elsevier.com/locate/structures

Performance evaluation of Natural Fiber Textile Reinforced Mortar (NFTRM) in masonry structural upgrading

Flavio Stochino [a,*], Arnas Majumder [a], Monica Valdes [a], Arumugaprabu Veerasimman [b], Mislav Stepinac [c], Enzo Martinelli [d]

[a] Department of Civil Environmental Engineering and Architecture, University of Cagliari, via Marengo 2, Cagliari, CA 09123, Italy
[b] Department of Mechanical Engineering, Kalasalingam Academy of Research and Education, Krishnankovil, 626126, India
[c] Faculty of Civil Engineering, University of Zagreb, Zagreb 10000, Croatia
[d] Department of Civil Engineering, University of Salerno, via Giovanni Paolo II n.132, Fisciano, SA 84084, Italy

ARTICLE INFO

Keywords:
Natural fiber textile-reinforced mortar
Jute
Masonry wall strengthening
In-plane cyclic shear
Sustainable retrofitting systems

ABSTRACT

Masonry buildings constructed in past centuries were generally built without seismic design provisions. Commonly, Fiber Reinforced Polymers (FRP) or Textile Reinforced Mortar (TRM) systems are used for masonry retrofitting/upgrading. TRM systems are generally considered more suitable for masonry upgrading applications. In this work, an experimental campaign has been developed to retrofit/upgrade masonry walls with a Natural Fiber (NF) TRM system configured with two jute fiber nets (mesh types: 2.5 cm×2.5 cm and 2.5 cm×1.25 cm), four jute fiber made diatons and/or jute fiber (1% fiber (30 mm) with respective to the mortar mass) composite Structural Mortar (SM). This paper reports the improved strength of masonry walls upgraded with the proposed NFTRM system. Constant vertical load has been applied on these upgraded walls, and the shear strength capacity and ultimate strength of these walls have been evaluated through in-plane cyclic shear tests. It has been found that the ultimate strength of the NFTRM system is found to be very close to each other and ranging between 2.7 (MPa) to 3.1 (MPa). The overall load-carrying capacity of the strengthened masonry walls increased by more than 455%. This study shows that jute-based NFTRM systems improve masonry performance while advancing sustainable, circular construction practices aligned with the United Nations Sustainable Development Goals.

1. Introduction

Structural strengthening of masonry buildings has become a very important issue in countries like Italy, which has a huge number of historical heritage buildings and a significant seismic load [1–3].

In recent years, Fiber Reinforced Polymer (FRP) composite systems [4–10] have been used for structural strengthening due to their high strength and durability [11,12]. At the same time due to known drawbacks and limitations of FRP systems, as highlighted in [13], inorganic matrix composites have been recently developed for masonry upgrade or retrofitting. These composite systems, generally referred to as either Textile Reinforced Mortar (TRM) [14], Fiber-Reinforcement Cementitious Matrix/Mortar (FRCM) [15], Textile Reinforced Concrete (TRC) [16], Fabric Reinforced Mortar (FRM) [17] and Inorganic Matrix-Grid (IMG) [18], consist of a textile matrix embedded within a layer of cement or lime-based mortar [19]

TRM systems (as they will be referred to hereinafter) are particularly suitable for upgrading and/or retrofitting the masonry structures [18]. Most commonly for TRM upgrading and/or retrofitting, man-made (organic, inorganic, and mineral) fibers like carbon fiber [20–22], glass fiber [23,24], basalt fiber [25,26], steel fiber [25–27], and polypropylene mesh [23] are commercially available, have been reported in the literature. These fibers are used due to their higher strength and durability [28].

In the construction and building sector, different applications of TRM for structural retrofitting/upgrading have been proposed in the literature. Recently Revanna and Moy (2024) [29] have studied the flexural behavior of the TRM (carbon and basalt fabric) strengthened concrete beam when subjected to extreme temperatures (200 °C-800°C). As reported by the authors degradation in flexural has been observed beyond 400°C. Notably, the TRMs can withstand temperatures up to 600°C. In [30] Mercimek et al. (2024) have strengthened different concrete columns using two types (meshes) of carbon textile and a special mortar (cement-based, fiber, and polymer-added mortar). Ultimate axial load

* Corresponding author.
E-mail address: fstochino@unica.it (F. Stochino).

https://doi.org/10.1016/j.istruc.2026.111742
Received 12 January 2026; Received in revised form 10 March 2026; Accepted 24 March 2026
Available online 31 March 2026

capacity was observed between 433.66 kN and 636.16 kN when compared with the reference sample (423.06 kN). In another case Gou et al. (2023) [31] have retrofitted different concrete columns using an optimized TRM (carbon textile, short polyvinyl alcohol (PVA) fiber) system. Notably the shear capacity improved by 54.3–55.2%. In an interesting case, Ramezani and Esfahani (2023) [32] have strengthened reinforced concrete beam specimens with the FRCM/TRM system, which is composed of carbon textile and cement-based repair mortar (recycled from industrial wastes). The load-carrying capacity was enhanced due to TRM strengthening by about 40 MPa on average (considering all reinforced samples) when compared with the reference sample. Interestingly, Campolongo et al. (2023) [33] have reinforced clay-brick masonry columns using polybenzoxazoles (PBO) TRM systems in various combinations. Improvement in axial strength was found from 5.96 MPa to 10.99 MPa considering all reinforced samples, and when 12.26 MPa was obtained for the reference sample. Glass fiber TRM has been used by Bertolesi et al. (2020) [34] to reinforce masonry cross vaults constructed following the technique of traditional Catalan layered construction. The structures were damaged, retrofitted, and tested to analyze their reaction to vertical support displacements. Based on the obtained overall results it has been reported that the TRM reinforcement can partially reinstate the initial stiffness, as well as double the vaults' elastic phase and ultimate displacements. Dong et al. (2021) [35] have retrofitted/upgraded unreinforced masonry walls using glass and carbon fiber TRM and carbon and glass TRM (one and both sides application) and with short and water-dispersible polyvinyl alcohol (PVA) fibers. Wall samples were subjected to diagonal compression tests, and improvement in load-bearing capacity from 60% to 412% (considering all retrofitting combinations). In-plane cyclic shear strength tests were performed on masonry walls with windows) retrofitted with a glass fiber TRM system, by Ivorra et al. (2021) [36]. Results have demonstrated an improvement in shear strength from about 120–300 kN, while the cumulative energy loss due to energy dissipation was observed around 2.7–12.7 kNm. Whereas, Furtado et al. (2020) [37] have upgraded masonry walls (hollow clay horizontal bricks) using polypropylene mesh, strong glass fiber mesh (GFRP), and M5 class mortar, whereas steel connectors were used to anchor the textile mesh. The out-of-plane tests have been conducted, while the flexural strength capacity and deformation capacity improved by 54% and 7.18 times, respectively. In another case, sample masonry walls are prepared with solid clay bricks (recycled from an early 20th-century building) and low-strength traditional mortar by Mezrea et al. (2021) [38]. Masonry walls were upgraded with carbon and basalt textile FRCM systems with and without anchors. Considering all retrofitting wall combinations, improvement in shear stress from 0.23 MPa to 0.95 MPa has been observed. Considering the recyclability of the building, in the last few years, researchers have studied integrated (structural and thermal) retrofitting schemes and they have used TRM for structural upgrading and insulation materials (mainly Expanded Polystyrene (EPS), and insulation mortars). Notably, Furtado et al. (2023) [39] have used a Glass-TRM system to retrofit masonry walls. Here authors have conducted the out-of-plane structural tests and reported improvements in the load-bearing capacity of the upgraded masonry wall samples from about 45–120%. Whereas Karlos et al. (2020) [40] have glass fiber TRM and EPS for seismic and energy upgrading of the masonry walls, and the obtained peak load improved from about 175–492%, considering all retrofitting combinations. Other interesting integrated (structural and thermal) masonry retrofitting can be in [41–43] and [44], in these cases, commercially available fabric has been used for TRM strengthening, whereas EPS has been used for thermal retrofitting.

These organic, inorganic, and mineral fibers contribute to environmental impacts throughout their life cycle, mainly due to greenhouse gas emissions associated with their production and disposal. Sometimes these fibers are harmful to human health [45]. Notably, the C&B sector is responsible for the emission of CO_2 and other CHG, about 39% globally and 36% in the European Union (EU). Further, as highlighted in [46], a third of the total waste generated in the EU is due to Construction and Demolition (C&D) activities, and it is about 180 tons of C&D waste per year [47]. To encourage sustainable development goals/strategy, the EU discourages 100% disposal of C&D wastes [48].

To reduce landfill waste and carbon footprint in the construction sector, more sustainable and biodegradable materials are needed. Research increasingly supports using natural fiber composites in TRM systems for masonry retrofitting, as they are recyclable, biodegradable, cost-effective, and can reduce carbon emissions by up to 79% [49] [50]. Considering the C&D application, some innovative research works and the use of natural (animal and plant) fibers like sheep wool [9,51], date palm fiber [52], oil palm fly ash fiber [53], Sisal fiber [54–59], hemp fiber [57,59,60], flax fiber [57,61,62], bamboo fiber [63,64], curauà fabric [65,66], kenaf fiber [67], alfa plant fiber [68] have been studied in the literature.

Nowadays, interest in the use of Natural Fiber (NF) TRM systems is increasing among scientists and researchers. Codispoti et al. (2015) [57] studied the mechanical performance of natural fiber-reinforced cementitious matrices (NFRCM). The authors have used jute, Sisal, hemp, and flax textiles, and inorganic nature mortar (prepared with pozzolana lime and natural siliceous) to prepare the TRM samples. Tensile strengths obtained for jute TRM, hemp TRM [69], and flax TRM were about 440 MPa (on average), 268 MPa, and 774 MPa, respectively. Tensile behavior of the flax and jute fiber TRM samples was tested by Trochoutsou et al. (2021) [70]. Obtained tensile strengths for flax-TRM and jute-TRM were found to be between 57.6 and 223.4 MPa, and 62.7–74.0 MPa, respectively. In another case, masonry walls were reinforced with the jute TRM system by Khaleel et al. (2021) [71]. The authors have applied jute textiles around the unreinforced walls. The mechanical tests showed compressive strength increases of about 10% for the reinforced English-bond prisms and 57% for the stack-bond prisms, while flexural strength improved by approximately 40% and 147%, respectively. In [65], Ferrara et al. (2021) have provided a comparative result (tensile response) between flax TRM composite specimens and flax TRM curauá fiber composite specimens. For the second composite combination, enhancement in stress and dissipated energy were observed of approximately 28% and 45%, respectively. Recently, Pepe et al. (2023) [72] have evaluated the tensile strengths of the Lime-Based jute TRM and Flax TRM specimens. The tensile strength obtained near about 1.2 MPa and 2.4 MPa for JTRM and FTRM, respectively.

There are some interesting studies available in the literature on the use of NFTRM systems for masonry upgrading/retrofitting. The structural behaviors of the diagonal compressive tests, of yellow tuff brick walls and solid clay brick walls reinforced with Hemp Fiber Composite (HFC) system in Menna et al. (2015) [73]. Notably, for reinforced purposes pozzolanic and HNL mortars, and HFC ties/connectors have been used. Improvement in peak shear stress values considering all types of upgraded yellow tuff brick walls obtained about 0.40 MPa, and this increment considering all types of solid clay brick walls was found to be about 0.69 MPa when compared with un-strengthened wall samples prepared with respective brick types. In Ferrara et al. (2020) [74] have utilized flax textile in two different combinations, single layer, and two layers to reinforce masonry walls. Structural behaviors were determined through the diagonal compression test. As reported, due to the application of the flax-TRM system the improvement in the peak load withstanding capacity was observed at approximately about 65 MPa (single layer) and 86 MPa (two layers), when compared with unreinforced masonry wall (64 MPa).

Jute fiber is the second most produced natural fiber [75]. In the last 57 years jute fiber production increased by 1 million tons. Notably around 6 million households engage with jute fiber production and the value of the jute fiber production is around 1.2 billion dollar [76]., there are many positive sides of jute plant cultivation, it improves the fertility of the soil, purifies the air by absorbing CO_2 and emitting O_2 [77]. The jute fiber production and its products require lower energy during their

production process and pose less hazard during manufacturing [78], when compared with man-made and mineral fibers. Notably, Jute fiber is known to be cheap, and recyclable, and also its strength and insulating capacity [79] [77] make it attractive and competitive as construction material. The jute fiber and its derived products are quickly gaining importance in the construction and building sector.

This paper investigates the retrofitting of masonry walls using jute fiber products, jute fiber nets, jute fiber diatons, and jute fiber composite mortar within a Natural Fiber Textile Reinforced Mortar (NFTRM) system. The mechanical performance of the upgraded walls is evaluated through in-plane cyclic shear tests. Therefore, the primary objectives of this experimental research campaign are to promote the use of natural fibers in green construction and to advance the circular economy. Further, this research provides some innovative compact and innovative NFTRM packages for masonry retrofitting/upgrading. Finally, this research advocates the United Nations Sustainable Development Goals.

2. Material and method

The research activity performed and presented in this paper (structural level) is a continuation of the authors' previous research works performed at:

(1) Fiber level: where physical (water absorption) and mechanical (tensile strength) performance of the jute fiber, jute fiber threads, and jute fiber diatons have been evaluated, see Majumder et al. (2022) [80].
(2) Mechanical level: during this phase various combinations of the jute fiber composite mortars are formulated, and their thermo-mechanical properties were evaluated [79]. Therefore, the flexural and compressive strength tests were performed, and the strain energy was calculated. Thermal conductivity tests were also performed on all mixture compositions, as our target was to choose a composite mixture with balanced mechanical and thermal (insulation) properties. This mixture has been used for the integrated (structural and thermal) retrofitting/upgrading (see, sub-2.8), for details see, Majumder et al. (2023) [79].

2.1. Raw Jute fiber

Fig. 1.a presents the jute plants of Bangla Tosha - *Corchorus olitorius* (golden shine) origin. The raw jute fibers (Fig. 1.b) derive from the inner bark [50] of these plants, they are approximately 3–4 m long. The fibers used in this research were collected directly from farmers in the state of West Bengal, India.

The physical properties and mechanical behavior of the jute fiber are reported in [80]. This jute fiber can absorb more than 200% of water with respect to its dry mass. Whereas the tensile strength and ultimate strain energy respectively are 215.11 MPa and 0.77 N.mm. The knowledge and results from the water absorption test [80] have been used as a guide while preparing the Structural Mortar (SM) composite sample and later the flexural and compression tests were performed on these composite samples [79].

The knowledge and results obtained in [80] and [79] have been used for the masonry upgrade reported in this paper. Only 30 mm long fiber (Fig. 2.a) has been used (motivations explained in 2.5) for the composite mortar layer of the NFTRM system.

2.2. Jute diatons

Fig. 3 presents the jute diatons fabricated in the structural laboratory of the University of Cagliari.

These transversal connectors have been used for the masonry wall upgrading to connect two surfaces of the NFTRM system and also to improve the wall shear capacity. Diatons preparation, physical properties, and mechanical behaviors are reported in [80], and their tensile strength and strain energy were found to be around 15.54 MPa and 14.18 kN.mm.

2.3. Jute thread and jute net fabrication

Two types (class 1 mm and class 2 mm, see [80]) of three yarn jute threads were collected from the same place of jute fiber. The class 1 mm (Fig. 4.a) thread was preferred and used for the net fabrication (Fig. 4.b) due to its higher mechanical performance [80].

Two different mesh configurations 2.5 cm × 2.5 cm (Fig. 5.a) and 2.5 cm × 1.25 cm (Fig. 5.b), respectively, were chosen for different net preparations. The jute fiber nets were fabricated with two different dimensions: (1) the 1 × 1 m^2 (Fig. 5. c&d)used for strengthening the masonry wall specimens used for structural tests and (2) the 0.9 × 0.7 m^2 (Fig. 5.d) used for strengthening the masonry wall specimens used for the thermal conduction tests not analyzed in this paper.

Fig. 6.a shows the jute fiber net tensile strength test preparation, while Fig. 6.b shows the tensile strength test conducted on a net sample of configuration 1.25 cm × 2.5 cm, using a universal machine of specifications: maximum load capacity of 630 kN, maximum workable length of 20 cm, rate of 2 mm/min. The test results are presented in

Fig. 1. (a) Jute plants and (b) Raw jute fibers.

Fig. 2. 6.5 g of raw jute fibers of (a) 30 mm, (b) 20 mm, and (c) 5 mm fiber lengths.

Fig. 3. Jute fiber made diatons.

Fig. 4. (a) Jute thread of class 1 mm and (b) Jute net preparation.

Table 1. For more details please see [47].

2.4. Structural mortar

A cement-based mortar referred to as "Structural Mortar" (SM) has been used for the masonry walls upgrade. It is classed as M10 class [81, 82]. Mechanical performance was evaluated using three-point bending tests conducted on a displacement-controlled machine (4.9 kN capacity, 0.02 kN sensitivity), while compression tests were conducted on a load-controlled machine (100 kN capacity). All tests were performed using EN 1015–11 standard [83]. Table 2 presents the mechanical properties of the SM mortars.

2.5. Composite mortar

The composite-SM, obtained by adding jute fibers (Fig. 7.a) to the mortar (Fig. 7.b) matrix along with an appropriate amount of water (Fig. 7.c), has been used for upgrading eight masonry walls, which have been used for structural tests. Table 3 presents the mixture composition of the composite mortar (Table 4).

2.6. Choice of jute fiber length and fiber percentages

The choice of fiber length, fiber percentage (with respect to the dry mortar masses), and the amount of water used in the mixture, was based on previous analysis reported in [79] and [80]. The mechanical properties of mixes with different combinations of fiber length and fiber percentage of SM are summarized in Table 1 (for details see Fig. 8 and [79]).

As reported in [79], it has been observed that with the application of jute fiber: (1) the flexural strength and compressive strength have been decreased, and (2) the improvement in strain energy and thermal insulation properties of the composite sample have been observed. The reduction in strength and the increase in strain energy are directly related to the fiber percentage used in the mixture (0.5%, 1.0%, 1.5–2.0%).

The decrement is due to the fact that the homogeneity of the mortar is altered by the addition of jute fiber. In the previous research, the authors observed that when raw jute fibers are exposed to water, they tend to form fiber balls. These balls behave somewhat like sponges by trapping water. Notably, it is difficult to completely eliminate water during sample preparation. When these samples dry, air voids are likely to form within the samples, thereby weakening their flexural and compressive strengths. However, it is worth noting that this air void also makes these specimens better insulating materials.

The composite mortars have been prepared by mixing 1% of jute fiber (of fiber length 30 mm) with SM with respect to the dry mortar masses. Whereas, about 20% of the water amount (with respect to total structural and jute fiber mass) has been used for the composite mortar preparation. This selection was due to:

(1) To have a composite mixture with a balanced and optimum thermo-mechanical behavior (as in Fig. 8.),
(2) Another point that has been considered while selecting 1% of fiber (with respect to the mortar mass) for the composite mixture, is based on [84] which states that the presence of fiber in an incombustible composite mixture should not be higher than 1%.

2.7. Bricks used and masonry wall

The semi-solid brick blocks /hollow bricks depicted in Fig. 9.(a) meet

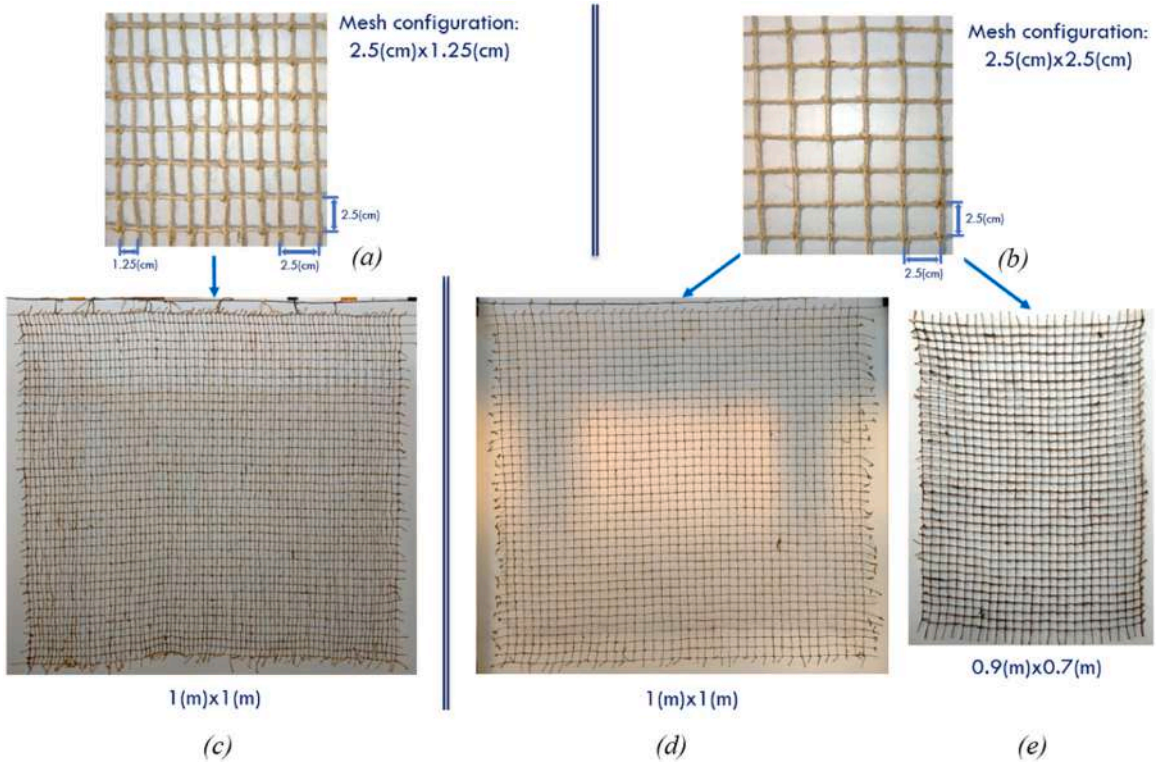

Fig. 5. Jute fiber nets.

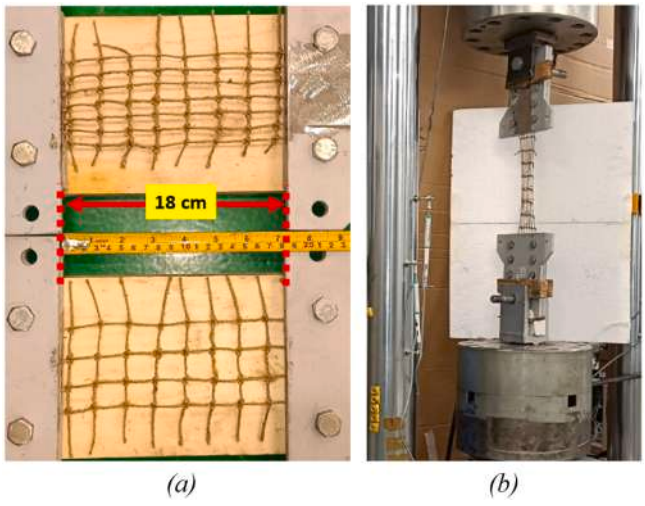

Fig. 6. (a) Net samples clamped for the tests, and (b) net tensile strength test.

Table 1
Mechanical properties of jute fiber net of configuration 2.5 cm × 2.5 cm see [47].

	Net of configuration: 1.25 cm × 2.5 cm	Net of configuration: 2.5 cm × 2.5 cm
Stiffness [N/mm]	10.3 (with CoV of 11.9%)	7.6 (with CoV of 20.2%)
Strain energy [kNmm]	14.1 (with CoV of 21.0%)	8.8 (with CoV of 39.1%)
Maximum load [N]	337.2 (with CoV of 9.9%)	217.3 (with CoV of 24.8%)
Maximum displacement [mm]	82.9 (with CoV of 18.6%)	72.5 (with CoV of 17.8%)

* CoV is Coefficient of Variation

Table 2
Mechanical performance [79].

Flexural properties	Stress	7.8 MPa (with Co.V. of 6.5%)
	Strain	0.013 (with Co.V. of 9.7%)
	Strain energy	0.19 (with Co.V. of 29.72%)
Compression property	Strength	32.25 MPa (with Co.V. of 5.61%)

* CoV is Coefficient of Variation

all requirements outlined in the "Technical Standards for Construction" (Ministerial Decree 17/01/2018) [81]. These bricks have the following specifications: dimension of 300 mm × 250 mm × 250 mm, and specific gravity of 800 ÷ 860 kg/m^3 [85]. They also meet additional criteria for masonry materials designed to withstand seismic activity, including straight and continuous partitions arranged parallel to the wall plane (with minor interruptions for gripping holes) and a vertical characteristic compressive strength of fBk $\geq$ 5 N/mm^2 and orthogonal compressive strength in the wall plane of f'Bk $\geq$ 1.5 N/mm^2. For reference, the dimensions of an un-strengthened, unreinforced hollow brick wall are depicted in Fig. 9.(b).

2.8. Masonry wall upgrading schemes for structural characterization

Two unreinforced and ten reinforced masonry Hollow Brick Walls (HBW), were constructed in the materials strength laboratory at the University of Cagliari. These walls were tested with various retrofitting/upgrading configurations, see Table 2. Two different vertical loads (40 kN and 80 kN) were applied in order to simulate different axial stress levels acting on masonry walls in real structures. These values correspond approximately to 1% and 2% of the estimated maximum vertical load capacity of the wall and were selected to investigate the influence of axial compression on the in-plane shear behaviour of both unreinforced and strengthened specimens.

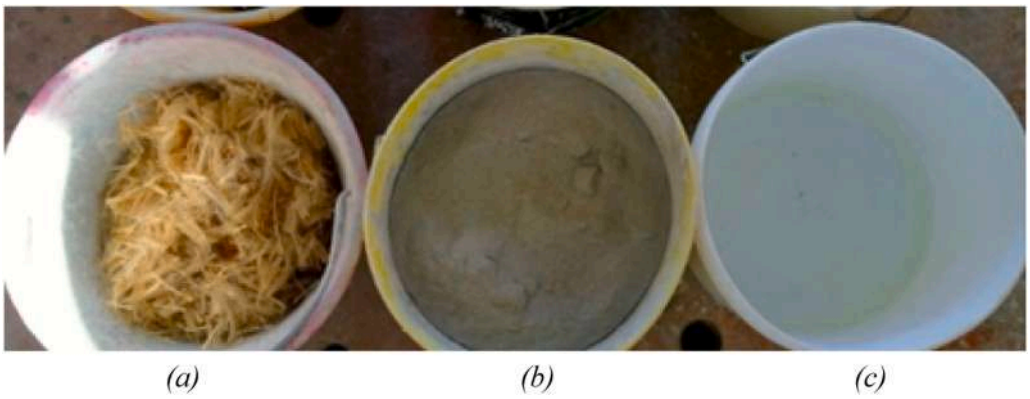

Fig. 7. Composite mortar preparation mixture ingredients: (a) 30 mm fiber, (b) SM and (c) water.

Table 3
Mixture composition.

Material used	Mixture proportion
Jute fiber (30 mm)	0.82%
SM mortar	81.06%
Water	18.12%

Table 4
Mechanical properties of mixes with different combinations of fiber length and fiber percentage of SM (based on results obtained in [79] and [80].

Best Value	Chosen value	Worst value
Stain energy [kN.mm]		
MSF2(30)	MSF1(30)	MS (No fiber)
2.687 (with CoV of 34.84%)	0551 (with CoV of 67.01%)	0.477 (with CoV of 13.90%)
Flexural stress [MPa]		
MS (No fiber)	MSF1(30)	MSF2(5)
7.789 (with CoV of 8.455%)	5.068 (with CoV of 7.93%)	3.611 (with CoV of 10.92%)
Compressive strength [MPa]		
MS (No fiber)	MSF1(30)	MSF2(30)
32.25 (with CoV of 5.61%)	21.83 (with CoV of 5.79%)	6.03 (with CoV of 7.47%)

Note: MS is the structural mortar; F represents the jute fiber, the number after F represents the percentage of jute fiber used in the composite mixture i.e., 1%, 2%, etc.; (30), (10), and (5) signifies the fiber lengths i.e., 30 mm, 10 mm, and 5 mm, respectively.
* CoV is Coefficient of Variation

- HBW1 (Fig. 10.a&c) and HBW2 (Fig. 10.b&d) masonry walls were not reinforced. Approximately 40 kN and 80 kN of constant vertical loads were applied to these masonry walls, respectively.
- Both HBW3 (Fig. 12.a) and HBW4 (Fig. 12.b) walls were reinforced with the jute net and jute diatons. Jute nets of 1 m^2 (of 2.5 cm × 2.5 cm mesh configuration) were placed on both sides of the masonry walls. In addition, four jute diatons (horizontal connectors passing through the wall thickness) were inserted orthogonally through the masonry walls (as in Fig. 13.a) to hold the nets connecting the external TRM layers (as in Fig. 13.c) and to improve the shear resistance. Thereafter, hollow cavities (of the inserted diatons) were filled with liquid mortar (Fig. 13.b). SM was used for binding the diatons, jute net attachment to the wall, and plastering. Vertical loads of approximately 80 kN and 40 kN were applied on HBW3 and HBW5, respectively.
- The masonry walls HBW5 and HBW6 have been reinforced with four diatons and jute nets with 2.5 cm × 1.25 mesh and 2.5 cm × 2.5 mesh configurations, respectively. Here too, the SM was used for the initial placement of jute fiber nets on both sides of HBW5 and HBW6.

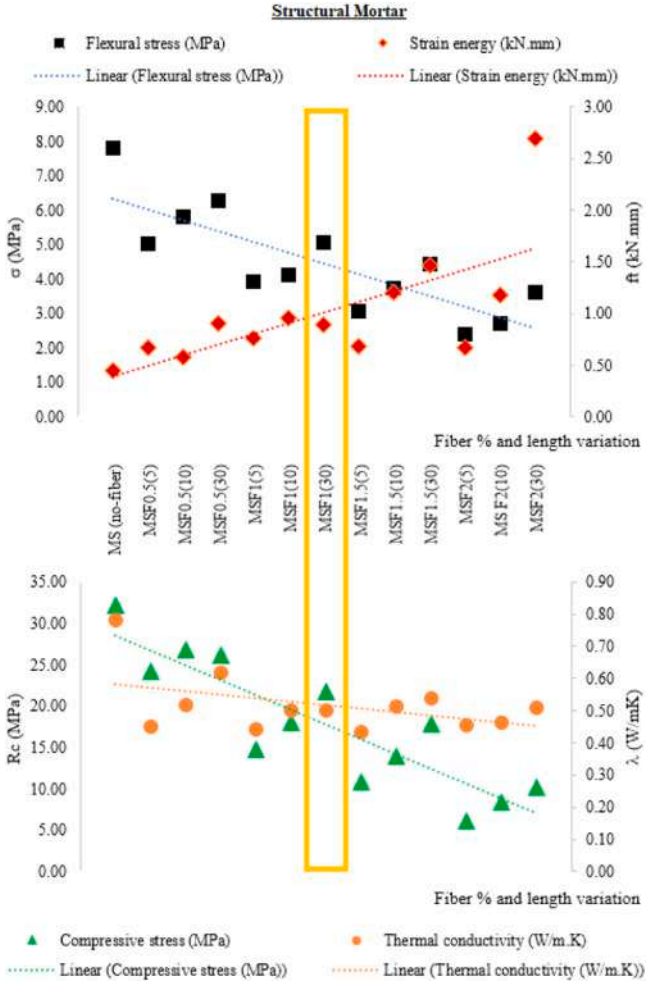

Fig. 8. The choice of 30 mm fibers and 1% fibers in the mixture with respect to the dry structural mortar (SM) mass, where Rc, ft, Rc, and λ, respectively, denote compressive strength, flexural strength, ultimate strain energy, and thermal conductivity.

Thereafter, jute-composite mortar prepared with 1% (with respect to the dry mortar mass) jute fiber and 30 mm fiber lengths was used for further thermo-structural reinforcement. 40 kN of constant vertical load was applied on both these masonry walls.

- The HBW7 has been reinforced with only 4 diatons. The diatons were bonded to the masonry wall surfaces using SM and the hollow cavities were filled with liquid mortar, as above.

Fig. 9. (a) Hollow bricks, and (b) reference wall sample (1 m x 1 m x 0.25 m).

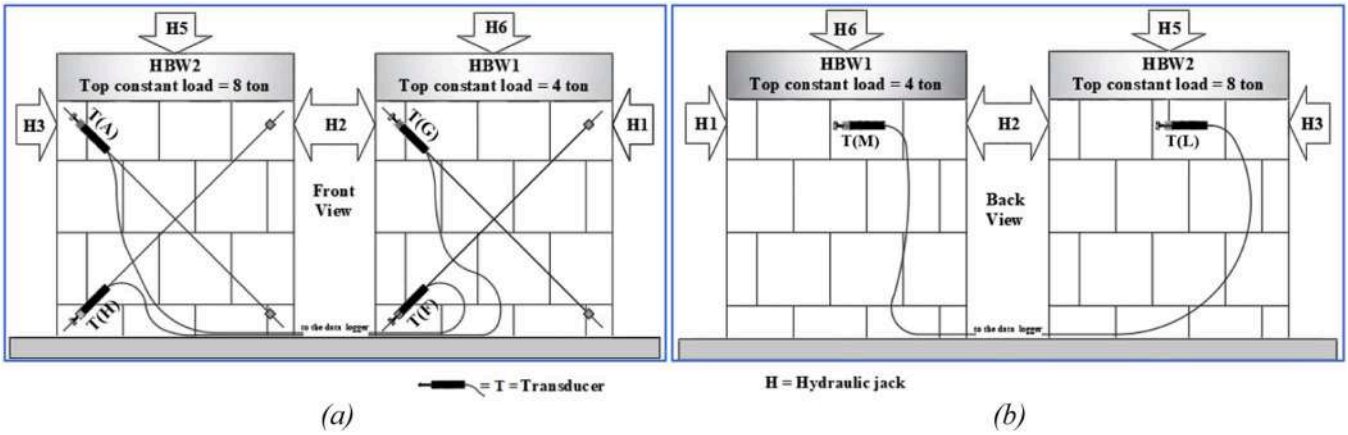

Fig. 10. Test setup: Masonry walls (HBW1 and HBW2) without reinforcement: (a) Front and (b) back views.

- In the case of masonry wall HBW8, raw jute fibers were placed diagonally and attached with SM on the wall surfaces, whereas four jute diatons were used to hold these fibers.

The quasi-static load protocol is defined as follows: first, the vertical load (about 2%: 80 kN and 1% 40 kN of the maximum vertical load of the wall) is applied. Subsequently, cyclic in-plane horizontal loads of increasing amplitude were introduced using three horizontal hydraulic jacks. The loading sequence began with the activation of jack H1 followed by H2 and H3, as illustrated in Fig. 10. Upon completion of the cyclic loading protocol, the wall's load-bearing capacity was evaluated by applying a final horizontal load through either jack H2 or H3, continuing until structural failure occurred. While H4 and H5 are the actuators, which have been used for applying fixed loads on the masonry walls.

Fig. 11.a represents the transversal diaton, while Fig. 11.b and Fig. 11.c respectively represent the structural mortar and composite mortar with 1% of jute fiber (1 mm). Fig. 11.d reports the raw jute fiber reinforcement scheme.

Fig. 12 represents various retrofitting/upgrading schemes of the masonry walls used for the in-plane cyclic tests. Fig. 12 (a) and (b) Fig. 12 (b) present the HBW3 and HBW4 masonry walls reinforced with jute net mesh (2.5 cm×2.5 cm) and 4 jute diatons. Whereas Fig. 12 (c) is the HBW5 Masonry walls reinforced with jute net mesh:

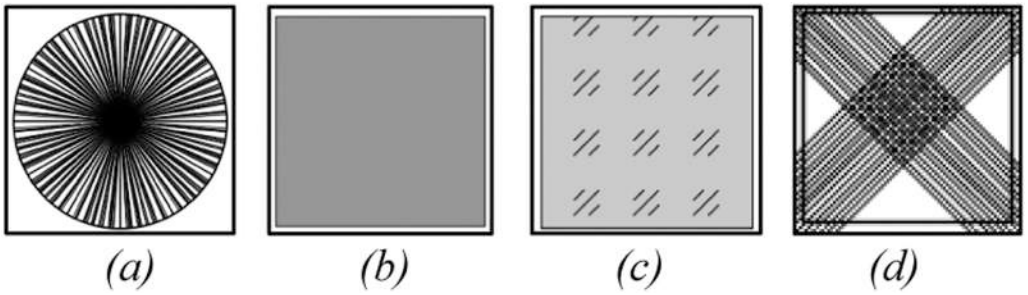

Fig. 11. (a) Transversal diaton, (b) Structural Mortar (SM) and (c) Jute composite mortar (SM) with 1 mm jute fiber (1% with respect to the mortar mass and (d) Raw intact jute fiber.

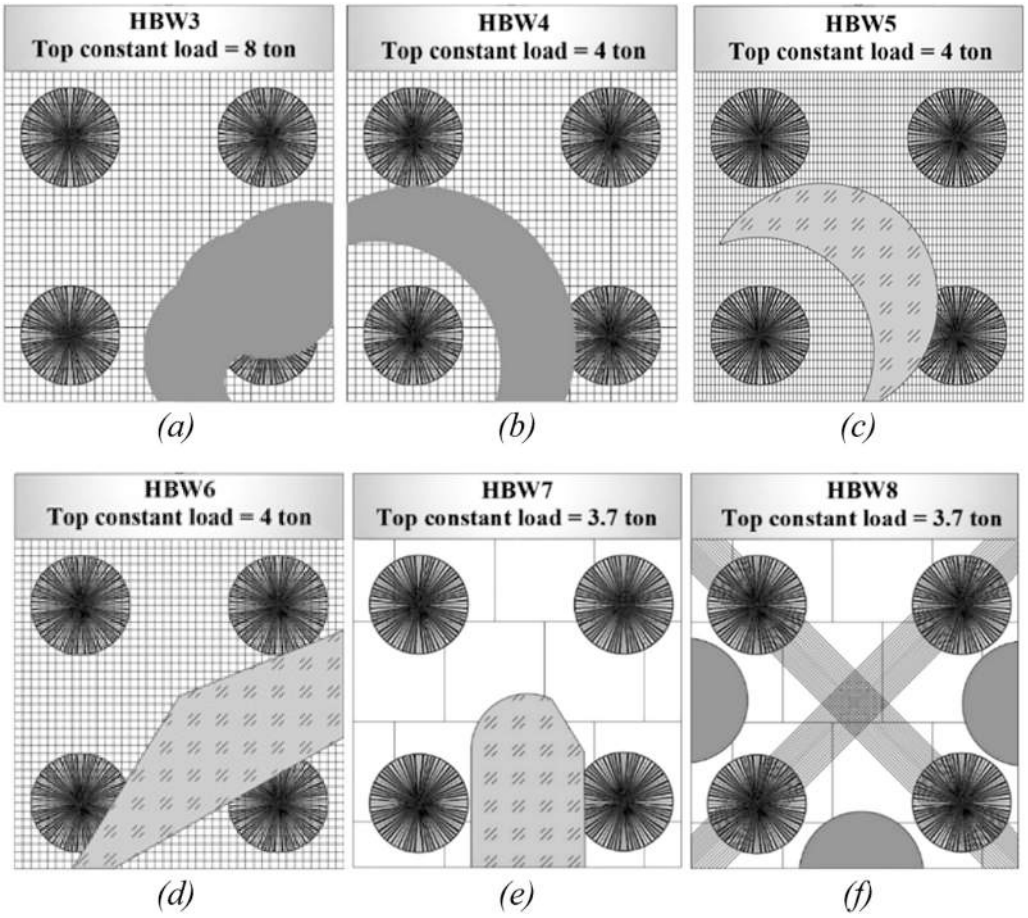

Fig. 12. Masonry walls: (a) HBW3, (b) HBW4, (c) HBW5, (d) HBW6, (e)HBW7, and (f) HBW8.

2.5 cm× 1.25 cm, 4 jute diatons, and jute composite SM. Fig. 12 (d) shows the masonry wall sample HBW6 retrofitted with jute net mesh: 2.5 cm× 2.5 cm, 4 jute diatons, and jute composite SM. While the masonry wall HBW7 has 4 jute diatons and jute composite SM (Fig. 12.e); and masonry wall HBW8 retrofitted with long intact raw jute fiber X pattern, 4 jute diatons.

The transversal diatons (Fig. 3) were placed through the wall holes (Fig. 13.a) and these holes were fully filled and sealed with liquid mortar (Fig. 13.b). Thereafter, the diaton edges (Fig. 13.c) (front and back) were opened and attached to the net (masonry wall surface) with SM.

Fig. 14 represents various steps of masonry wall upgrading schemes. Four holes are drilled through all masonry wall (Fig. 14.a). Four jute fiber diatons are placed through all masonry walls (Fig. 14.b). Application of diatons on the masonry wall HBW7 (Fig. 14.c). Whereas, Fig. 14.d and Fig. 14.e presents the masonry wall HBW3 installed with jute nets of 2.5 cm × 2.5 cm mesh configuration and HBW5 installed with jute nets of 2.5 cm × 2.5 cm mesh configuration.

It is important to highlight that all masonry walls were built together. The un-retrofitted masonry walls were subjected to the in-plane cyclic tests after 28 days of curing under normal environmental conditions. Whereas all other walls were retrofitted/upgraded together after 3 days from the day of construction, and they were tested after 28 days from the day of retrofitting/upgrading.

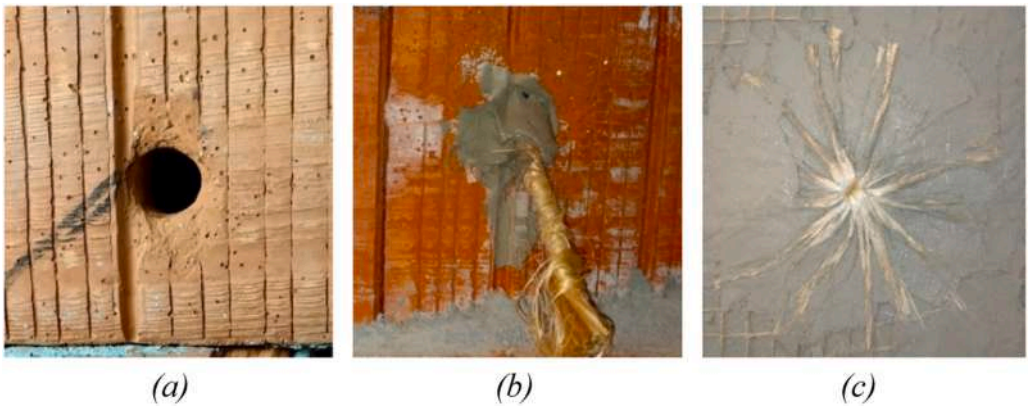

Fig. 13. (a) Transversal diaton hole, (b) transversal jute diaton, and (c) diaton holding net.

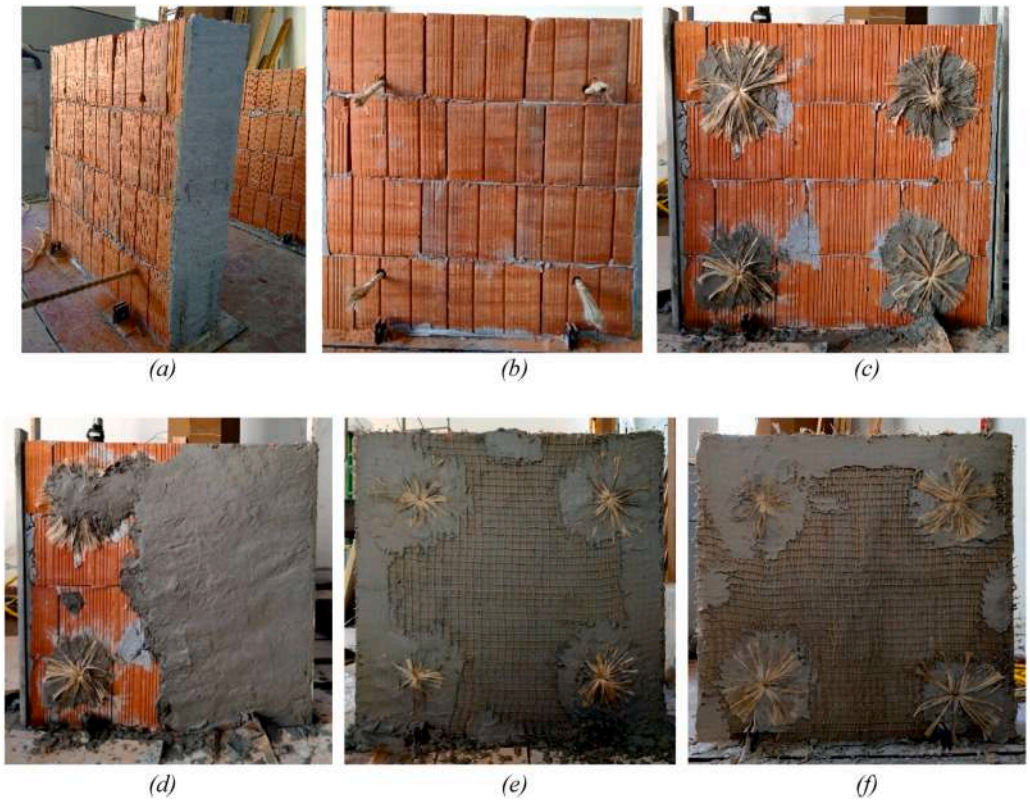

Fig. 14. Retrofitted/upgraded masonry walls: (a) Drilling transversal holes, (b) diatons placed through the masonry wall, (b) diatons are installed and fixed on the masonry wall, (c) application of composite mortar on the masonry wall, (d) jute net (2.5 cm × 2.5 cm mesh configuration) and jute diaton application on masonry wall, and (e) jute net (1.25 cm × 2.5 cm mesh configuration) and jute diaton application on masonry wall.

3. Experimental results

3.1. Upgraded masonry walls for structural characterization

3.1.1. In-plane cyclic shear tests

A total of 8 samples were used for the in-plane cyclic shear test. During these tests, a constant vertical load was applied at the top of each masonry wall, while the in-plane cyclic horizontal loads were applied using a set of hydraulic jacks.

Each wall was subjected to two or three cycles of growing horizontal loads from the right (hydraulic jack H1 or hydraulic jack H2 depending on the side of the considered wall) and from the left (hydraulic jack H2 or H3 depending on the side of the considered wall) (Fig. 10). At the end of the horizontal load cycles an increasing horizontal load was applied until the collapse of the sample. Each wall was equipped with three displacement Transducers (T) that convert rectilinear mechanical motion into a variable electric signal that can be digitally recorded. Their nominal displacement is 100 mm, nominal sensitivity 2 mV/V, sensitivity tolerance ± 0.1%, measure resolution 1 μm. Their positions are also represented in Fig. 10.a&b and Fig. 15.a: two are placed on the front surface to measure diagonal displacements while one is placed on the back surface to record horizontal displacements on every masonry wall, as shown in Fig. 10.c&d and Fig. 15.b, respectively.

Fig. 16 to Fig. 23 presented load-displacement curves for wall samples HBW1, HBW2, HBW3, HBW4, HBW5, HBW6, HBW7, and HBW8, respectively.

In all Figs. (16–21)), the red curves represent the first load cycle (C1), while the black curves denote the second load cycle (C2) and the green curves represent the third load cycle (C3). Displacements can be negative or positive depending on the direction of the acting forces.

3.1.1.1. Masonry wall sample: HBW1. HBW1 denotes a simple unreinforced brick masonry wall. Its vertical load is kept constant and equal to 40 kN while its load-displacement behavior is reported in Fig. 16.(a) for

Fig. 15. Samples equipped at the (a) front with diagonal sensors and (b) back with horizontal sensors.

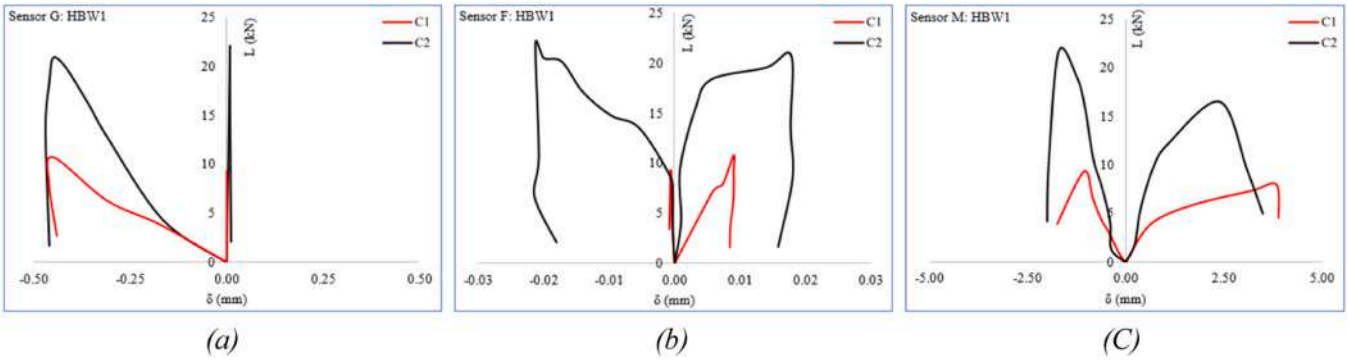

Fig. 16. Load-displacement diagrams of the unreinforced masonry wall HBW1, measured with (a) the diagonal sensor G, (b) the diagonal sensor F, and (c) the horizontal sensor M.

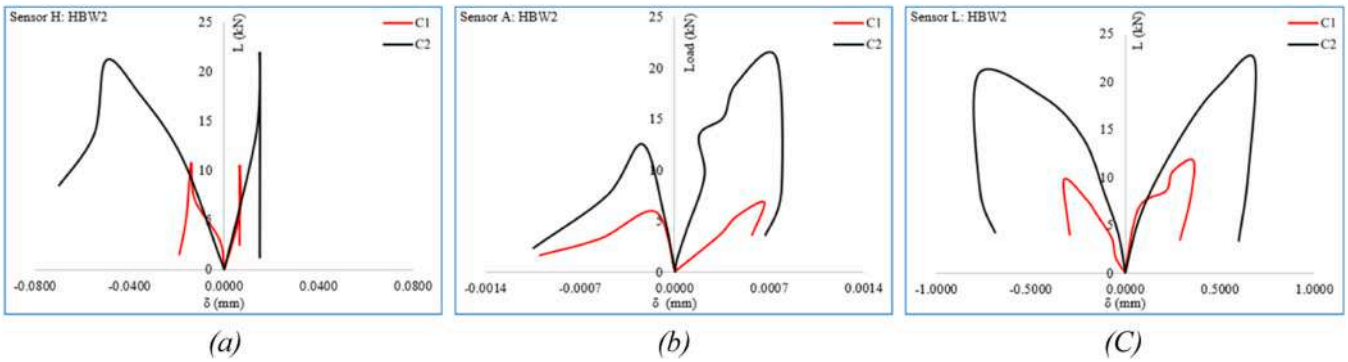

Fig. 17. Load-displacement diagrams of the unreinforced masonry wall HBW2, measured with (a) the diagonal sensor A, (b) the diagonal sensor H, and (c) the horizontal sensor L.

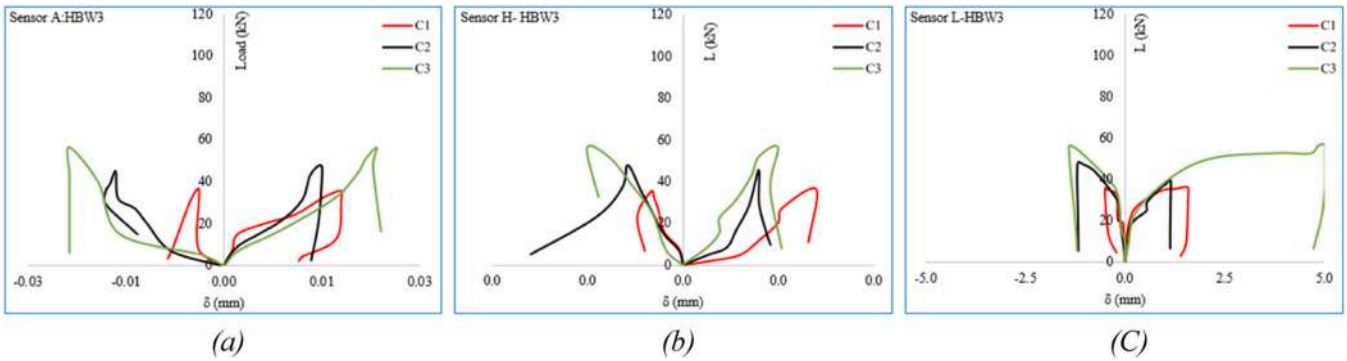

Fig. 18. (a) Load-displacement diagrams of the reinforced masonry wall HBW3, measured with (a) the diagonal sensor A, (b) the diagonal sensor H, and (c) the horizontal sensor L.

diagonal displacement Transducer T(G) and Fig. 16.(b) for diagonal displacement Transducer T(F). Whereas, Fig. 16.(c) presents the load-displacement relationship based on the horizontal displacement Transducers T(M).

Fig. 16 related to displacement transducer G, a good symmetrical behavior has been recorded for HBW1. The small asymmetry in Fig. 16.(c) can be explained by some error in the sensor placement.

3.1.1.2. Masonry wall sample: HBW2. HBW2 denotes another not-reinforced brick masonry wall. The difference with respect to HBW1 is in the vertical load that it is kept constant and equal to 80 kN. Load-displacement behavior is reported Fig. 17.(a) for diagonal displacement transducer T(A) and Fig. 17.(b) for diagonal displacement transducer T(H). Whereas Fig. 17.(c) presents the load-displacement relationship based on the horizontal displacement transducers labeled T(L)

A symmetrical behavior has been recorded, while the diagonal sensors A and H produced quite different recordings when the horizontal load pushed the wall from left to right or vice versa. Probably also in this case the diagonal sensor placements were not perfect.

3.1.1.3. Masonry wall sample: HBW3. HBW3 sample was reinforced with the jute-net and jute diatons. Jute nets of 1 m^2 (of 2.5 cm×2.5 cm mesh configuration) were placed on either side of the wall, while four jute diatons (horizontal connectors) were inserted orthogonally. In this case, the vertical load is kept constant and equal to 80 kN. Load-displacement behavior is reported in Fig. 18.(a) for diagonal displacement transducer T(A) and Fig. 18.(b) for diagonal displacement

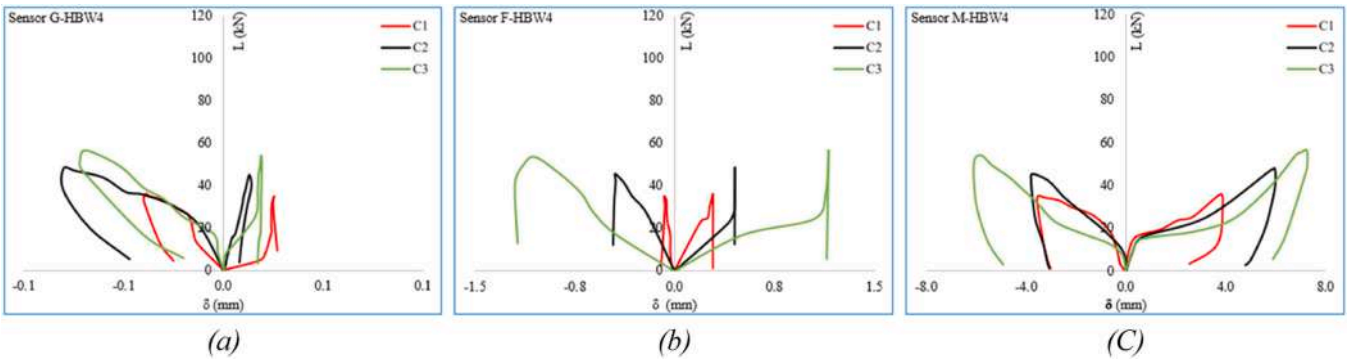

Fig. 19. Load-displacement diagrams of the reinforced masonry wall HBW4, measured with (a) the diagonal sensor G, (b)the diagonal sensor F, and (c) the horizontal sensor M.

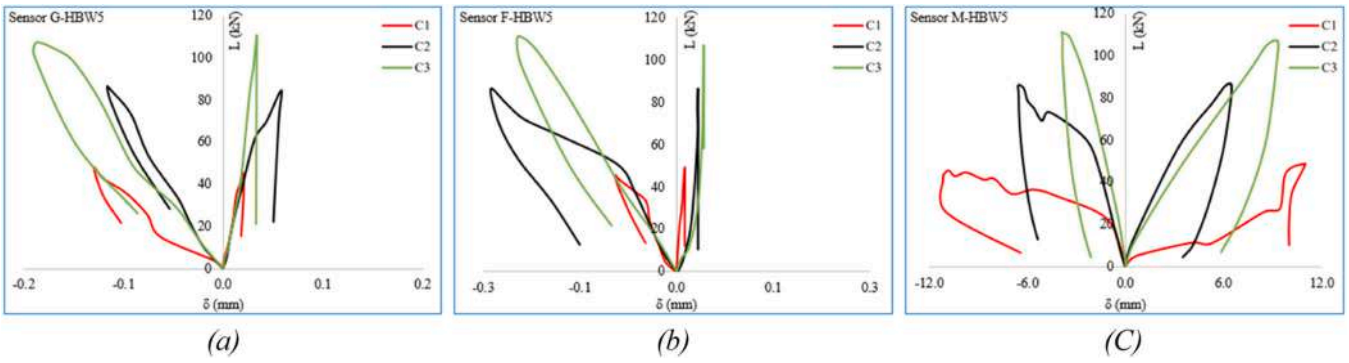

Fig. 20. Load-displacement diagrams of the reinforced masonry wall HBW5, measured with (a) the diagonal sensor G, (b) the diagonal sensor F, and (c) the horizontal sensor M.

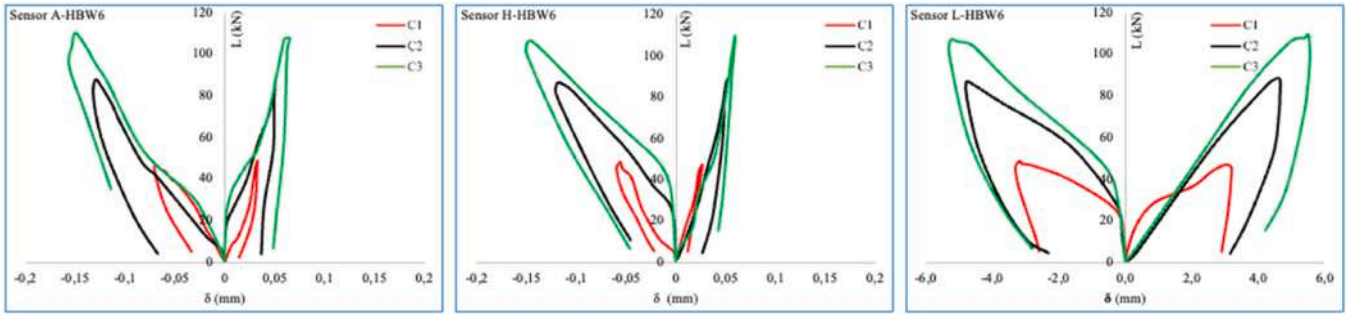

Fig. 21. Load-displacement diagrams of the reinforced masonry wall HBW6, measured with (a) the diagonal sensor A, (b)the diagonal sensor H, and (c) the horizontal sensor L.

transducer T(H). Fig. 18.(c) presents the load-displacement relationship based on the horizontal displacement transducers labelled T(L).

A quite symmetrical behavior has been recorded in all three above-mentioned figures apart from the last load cycle that yields to quite large horizontal displacements. In the latter case, small boundary modifications at the base of the wall can justify this difference in comparison to other load cycles.

3.1.1.4. Masonry wall sample: HBW4. HBW4 sample was reinforced with the jute-net and jute diatons. Jute nets of 1 m^2 (of 2.5 cm×2.5 cm mesh configuration) were placed on either side of the wall, while four jute diatons (horizontal connectors) were inserted orthogonally. In this case, the vertical load is kept constant and equal to 40 kN. Load-displacement behavior is reported in Fig. 19.(a) for diagonal displacement transducer T(G) and Fig. 19.(b) for diagonal displacement transducer T(F). Fig. 19.(c) presents the load-displacement relationship based on the horizontal displacement transducers labeled T(M).

3.1.1.5. Masonry wall sample: HBW5. Specimen HBW5 was reinforced with four transversal diatons and jute fiber nets on both sides with the 2.5 cm× 1.25 mesh configuration. Thereafter jute-composite structural mortar prepared with 1% (with respect to the dry mortar weight) jute fiber and 30 mm fiber lengths was used for further thermo-structural reinforcement. 40 kN of constant vertical load was applied on this wall. The load-displacement relationship is reported in Fig. 20.(a) for diagonal displacement transducer T(G) and Fig. 20.(b) for diagonal displacement transducer T(F). Fig. 20.(c) presents the load-displacement relationship based on the horizontal displacement transducers labeled as T(M).

Displacements can be negative or positive depending on the direction of the acting forces. The structural behavior of the wall has not been symmetric in all cases. Minor inaccuracies in sensor placement can

explain the differences between the positive and negative displacement zones in the above-mentioned Figures.

3.1.1.6. Masonry wall sample: HBW6. Specimen HBW6 was reinforced with four transversal diatons and jute fiber nets on both sides with the 2.5 cm× 2.5 mesh configuration. Thereafter, jute-composite structural mortar prepared with 1% (with respect to the dry mortar weight) jute fiber and 30 mm fiber lengths was used for further thermo-structural reinforcement. 40 kN of constant vertical load was applied on this wall.

The load-displacement relationship is reported in Fig. 21(a) for diagonal displacement transducer T(A) and Fig. 21(b) for diagonal displacement transducer T(H). Fig. 21(c) presents the load-displacement relationship based on the horizontal displacement transducers labeled as T(L).

3.1.1.7. Masonry wall sample: HBW7. Sample HBW7 has been reinforced with only 4 diatons to connect the external surfaces to improve the shear resistance. The diatons were bonded to the masonry wall surfaces using fiber-reinforced SM. 37 kN of constant vertical load was applied and kept constant on this wall.

The load-displacement relationship is reported in Fig. 22.(a) for diagonal displacement transducer T(G) and Fig. 22.(b) for diagonal displacement transducer T(F). Whereas, Fig. 22.(c) presents the load-displacement relationship based on the horizontal displacement transducers labeled T(L). The structural behavior of the wall has been almost symmetric in all cases except in Fig. 22.(b).

3.1.1.8. Masonry wall sample: HBW8. Sample HBW8 was reinforced with four transversal diatons and raw jute fibers were placed diagonally and attached with SM on the wall surfaces. 37 kN of constant vertical load was applied and kept constant on this wall.

The load-displacement relationship is reported in Fig. 23.(a) for diagonal displacement transducer T(A) and Fig. 23.(b) for diagonal displacement transducer T(H). Whereas, Fig. 23.(c) presents the load-displacement relationship based on the horizontal displacement transducers labeled as T(M). After the first load cycle, the structural behavior of the wall has not been symmetric, probably there has been a modification of wall boundary conditions (Table 5).

3.1.2. Maximum load

After the above-described load cycles, each wall has been subjected to an increasing horizontal load in order to measure the specimen capacity. Fig. 24 presents the load-displacement curves and highlights that the natural TRM system used for masonry upgrade i.e., the strengthened walls has shown better performance than that of hollow brick normal/un-reinforced walls. Table 6 summarizes the maximum loads and the corresponding displacement points for each wall. The overall withstanding load capacity of the strengthened masonry walls with the NFTRM system has increased by more than 455.66%.

The differences observed among the upgraded configurations can be explained by the combined effects of reinforcement geometry, mortar composition, and transverse connection. In particular, the mesh size of the jute net influences the density of the reinforcement and, consequently, the ability of the system to redistribute tensile stresses and control crack propagation. A denser mesh is expected to promote a more uniform stress transfer and a more distributed cracking pattern. The presence of the jute-fiber composite mortar layer further improves the interaction between reinforcement and masonry substrate, enhancing mechanical interlock, bond effectiveness, and the capacity of the strengthening system to engage a wider portion of the wall surface. In addition, the jute diatons play an important role in connecting the two external reinforced layers through the wall thickness, thereby limiting local detachment and improving the overall integrity of the strengthened system. The experimental results suggest that the improved performance of the NFTRM-upgraded walls is therefore governed by the synergistic interaction between mesh configuration, composite mortar layer, and diaton connection rather than by a single parameter alone.

3.1.3. Theoretical ultimate strengths of the upgraded masonry walls

In this case, only four strengthened masonry walls HBW3, HBW4, and HBW5 were considered, considering all these walls were upgraded the NFTRM system consisting of jute nets and jute fiber diatons. While HBW5 has an outer jute fiber composite layer.

Since Natural Fiber (NF) is used for upgrade purposes, the Natural Fiber TRM system will be called the NFTRM system hereafter.

According to a well-established approach in [18], the shear capacity of the strengthened wall, $V_{t,R}$ could be determined by calculating the minimum shear capacity of the unreinforced masonry wall, V_t and the contribution of the NFTRM, $V_{t,f}$ and summing these two values:

$$V_{t,R} = V_t + V_{t,f} \quad [\text{kN}] \tag{1}$$

where the two terms on the right-hand side can be expressed as follows:

the mechanical parameter characterizing the term V_t can be calculated by considering the results of the experimental tests carried out on the reference (un-strengthened) specimens (for the value see Table 10). While according to the Italian Building Code [81], V_t can be calculated using Eq. (2):

$$V_t = H \cdot t \cdot \frac{1.5}{p} \tau_{0d} \sqrt{\left(1 + \frac{\sigma_0}{1.5\ \tau_{0d}}\right)} \quad [\text{kN}] \tag{2}$$

where the length *(H)*, height *(l)* and thickness *(t)* of the solid clay brick masonry wall are equal to 1000 mm, 1000 mm and 200 mm, respectively.

Conversely, p is a correction coefficient of the stresses in the cross section, the maximum value i.e., 1.5 has been considered.

The stress due to vertical load (F_{top}) is a fixed load (Table 7) and it has been selected based on authors previous experimental experiences.

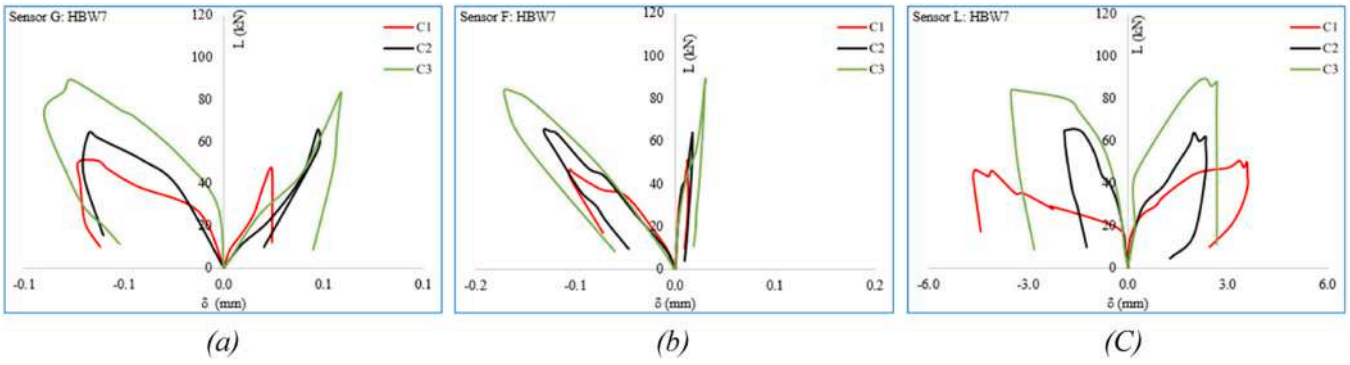

Fig. 22. Load-displacement diagrams of the reinforced masonry wall HBW7, measured with (a) the diagonal sensor G, (b) the diagonal sensor F, and (c) the horizontal sensor L.

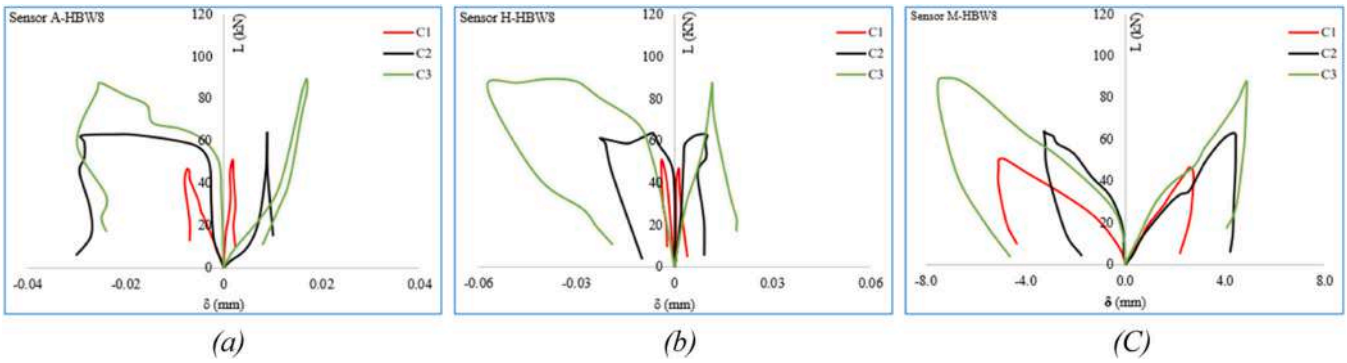

Fig. 23. Load-displacement diagrams of the reinforced masonry wall HBW8, measured with (a) the diagonal sensor A, (b) the diagonal sensor H, and (c) the horizontal sensor M.

Table 5
Masonry walls upgrading schemes.

Masonry wall nomenclatures	First mortar layer	Net Type	Total net used	Mesh type	Number of Diatons	Composite mortar used	Second mortar layer
HBW1 (1 m × 1 m × 0.25 m)	SM	no	no	no	no	no	SM
HBW2 (1 m × 1 m × 0.25 m)	SM	no	no	no	no	no	SM
HBW3 (1 m × 1 m × 0.280 m)	SM	1 m × 1 m	2	2.5 cm × 2.5 cm	4	no	SM
HBW4 (1 m × 1 m × 0.280 m)	SM	1 m × 1 m	2	2.5 cm × 2.5 cm	4	no	SM
HBW5 (1 m × 1 m × 0.285 m)	SM	1 m × 1 m	2	1.25 cm × 2.5 cm	4	SM + 1% (30 mm) jute fiber w.r.t. mortar mass	
HBW6 (1 m × 1 m × 0.285 m)	SM	1 m × 1 m	2	2.5 cm × 2.5 cm	4	SM + 1% (30 mm) jute fiber w.r.t. mortar mass	
HBW7 (1 m × 1 m × 0.280 m)	SM used only to fix diatons	no	no	no	4	SM + 1% (30 mm) jute fiber w.r.t. mortar mass	
HBW8 (1 m × 1 m × 0.280 m)	SM used only to fix diatons	no	no	no	4	no	SM

σ_0(MPa) the average normal stress can be calculated (Table 7) using the following Eq. (3):

$$\sigma_0 = \frac{F_{top}[N]}{H \cdot t[mm^2]} \quad (3)$$

The shear stress capacity due to vertical load i.e. τ_{0d} (MPa) could be computed (see Table 8) using Eq. (2) based on the assumption that V_t equal to the measured experimental value ($V_{t\ exp}$).

Interestingly, the calculated τ_{0d} (MPa) value (see the Table 8) of both un-upgraded masonry was found to fall in-between the range 0.10 – 0.13 [MPa] of the semi-hollow brick wall (i.e., Masonry with semi-solid clay bricks, with dry vertical joints (holes percentage < 45%).) as provided in the Italian NTC18 [81].

The overall contribution of the masonry wall, V_t was re-calculated by averaging the two parameters i.e., τ_{0d} and σ_0 and subsequently applying Eq. (1). The resulting value was determined to be 38.01 [kN].

The mechanical parameter characterizing the term $V_{t,f}$ represents the contribution of the NFTRM system and can be calculated according to the Italian Building Code [81] using Eq. (4):

$$V_{t,f} = \frac{1}{\gamma_{Rd}} . n_f . t_{vf} . l_f . \alpha_t . \varepsilon_{fd} . E_f \quad [\text{kN}] \quad (4)$$

Where the partial safety factor, γ_{Rd} is considered to be equal to 1, n_f represents the total number of the reinforced layers arranged at each side of the wall, as both sides of the masonry walls have been retrofitted, therefore n_f is equal to 1. The equivalent thickness t_{vf} is of a single layer of the NFTRM system is measured manually, l_f is the design dimension of the reinforcement measured orthogonally to the shear force, it can't be longer than the length of the masonry wall. Therefore $l_f \leq H$ and is equal to 1000 mm for all the specimens. α_t is the coefficient to account for the reduced tensile strength of fibers when under shear stress. According to [18] this value is assumed to equal to 0.80. E_f is the Young's/elastic modulus of elasticity of dry fabric/textile. ε_{fd} is the design strain of NFTRM. So, the design strength of the TRM system is:

$$\sigma_{fd} = \varepsilon_{fd} . E_f \quad [\text{MPa}] \quad (5)$$

Therefore, the Eq. (2) can be re-written as:

$$V_{t,f} = \frac{1}{\gamma_{Rd}} . n_f . t_{vf} . l_f . \alpha_t . \sigma_{fd} \quad [\text{kN}] \quad (6)$$

While the contribution of the NFTRM system, $V_{t,f}$ should be equal to:

$$V_{t,f} = V_{t,R} - V_t \quad [\text{kN}] \quad (7)$$

The shear capacity of the strengthened wall ($V_{t,R}$) should be equal to the measured experimental value of the maximum horizontal force ($V_{t,R\ exp.}$) resisted by the strengthened masonry wall.

See Table 9 for the values of $V_{t,R.\ exp.}$ for all upgraded masonry walls. While the value $V_{t.\ exp.}$ of the un-strengthened masonry wall is experimentally known, see Table 8.

Notably in the measured $V_{t,R\ exp.}$, is also included the contribution of the "2" NFTRM systems, therefore the TOTAL contribution can be calculation can be calculated as:

$$V_{t.f.TOTAL} = V_{t,R\ exp.} - V_{t.\ exp.} \quad [\text{kN}] \quad (8)$$

The authors assume that the NFTRM systems applied on each side of the masonry wall, have contributed equally to improve the overall strength (load bearing capacity) of the upgraded masonry wall.

Therefore, contribution of the singular TRM system can be calculated

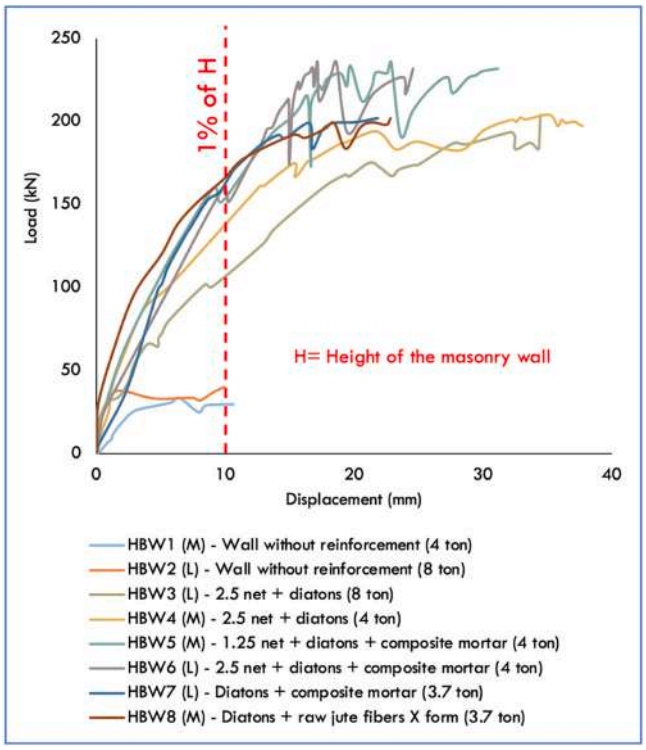

Fig. 24. Load-displacement graph, when the collapse load was applied (Horizontal sensors). The vertical red line identifies the 1% drift value.

Table 6
Applied horizontal collapse load and displacements.

Masonry wall	Load max [kN]	Corresponding displacement [mm]	Max displacement [mm]
HBW1 (Sensor-M)	35.41	11.12	11.12
HBW2 (Sensor-L)	40.00	9.88	9.88
HBW3 (Sensor-L)	204.07	34.46	34.46
HBW4 (Sensor-M)	204.17	35.15	37.70
HBW5 (Sensor-M)	235.47	22.87	31.15
HBW6 (Sensor-L)	236.21	17.14	24.57
HBW7 (Sensor-L)	201.97	21.82	21.82
HBW8 (Sensor-M)	201.87	22.82	22.82

Table 7
Fixed top load and average normal stress of the un-upgraded masonry walls.

	Fixed top load	Average normal stress
	F_{top} [N]	σ_0 [MPa]
HBW2(8ton)	79680	0.3984
HBW1(4ton)	39840	0.1992

Table 8
measured and calculated values of the un-strengthened masonry walls.

	Experimental maximum horizontal force	Shear stress capacity
	$V_{t\ exp}$ [kN]	τ_{0d} [MPa]
HBW2(8ton)	400.00	0.1073
HBW1(4ton)	354.10	0.1227

Table 9
The experimental and calculated values of the NFTRM system strengthened masonry walls.

	Experimental value of the maximum horizontal force	Total NFTRM contribution (calculated using)	Contribution of a single NFTRM system package (Calculated using)
	$V_{t,R,exp.}$ [kN]	$V_{t,f\text{-}TOTAL}$ [kN]	$V_{t,f}$ [kN]
HBW3 (8 ton)	204.07	166.06	83.03
HBW4 (4 ton)	204.17	166.16	83.08
HBW5 (4 ton)	235.47	197.46	98.73
HBW6 (4 ton)	236.21	198.20	99.10

using the Eq. 9.

$$V_{t,f} = \frac{V_{t,f.TOTAL}}{2} \quad [\text{kN}] \tag{9}$$

In fact, if $\varepsilon_{u,f}$ denotes the ultimate strain of the TRM system its ultimate strength is equal to:

$$\sigma_{u,f} = \quad \varepsilon_{u,f}. \quad E_f \quad [\text{MPa}] \tag{10}$$

By modifying the Eq. (6) to assess the ultimate limit state capacity and using the Eq. (10), the contribution of a single NFTRM system can be calculated:

$$V_{t,f} = \frac{1}{\gamma_{Rd}}.n_f.t_{vf}.l_f.\alpha_t.\sigma_{u,f} \quad [\text{kN}] \tag{11}$$

Therefore, the ultimate strength of a single NFTRM system could be calculated (Tables 10 and 11) as:

$$\sigma_{u,f} = \frac{V_{t,f}}{\frac{1}{\gamma_{Rd}}.n_f.t_{vf}.l_f.\alpha_t} = \frac{V_{t,R} - \quad V_t}{\frac{1}{\gamma_{Rd}}.n_f.t_{vf}.l_f.\alpha_t} \quad [\text{MPa}] \tag{12}$$

Interestingly, the obtained ultimate strengths of the NFTRM system are very close to each other, ranging from 2.7 to 3.1 MPa (see Table 10.

The ultimate strength of the NFTRM system on HBW5 (retrofitted with jute nets (2.5 cm × 1.25 cm), jute diatons, and jute fiber composite SM with 1% fiber (30 mm) with respect to the mortar mass) is found to be equal to around 2.90 (MPa). Whereas, the ultimate strength of the NFTRM system on HBW6 (retrofitted with jute nets (2.5 cm × 2.5 cm), jute diatons, and jute fiber composite SM with 1% fiber (30 mm) with respect to the mortar mass) is found to be equal to around 3.1 (MPa). HBW3 and HBW4 don't have any composite layers, and the ultimate strength of the NFTRM on these two specimens was found to be about 2.77 (MPa).

Therefore, it can be said that the presence of jute fiber composite layers in the NFTRM system has increased its ultimate strength by 4.8–8.3%.

Table 10
The ultimate strengths of the TRM system of the tested masonry walls.

	Mesh gap	Equivalent thickness of a single layer of the NFTRM system	Ultimate strength of a single NFTRM system (calculated using)
	[mm]	t_{vf} [mm]	$\sigma_{u,f}$ [MPa]
HBW3 (8 ton)	25.0	37.5	2.768
HBW4 (4 ton)	25.0	37.5	2.769
HBW5 (4 ton)	12.5	42.5	2.904
HBW6 (4 ton)	25.0	40.0	3.097

Table 11
Comparative summary of in-plane load capacity improvements reported for masonry wall strenghtened with various fiber-reinforced mortar systems.

Study	Strengthening Material	Test Type	Reported Maximum Load / Improvement	Reference
Present Study (NFTRM)	Jute nets + jute diatons + jute composite mortar (Industrial brick masonry wall)	In-plane	201.87 – 235.47 kN (≈ +455%)	This study
Ivorra et al. (2021)	Glass (Industrial bricks masonry wall with window)	In-plane	+ 110.86 kN	[36]
Mercedes et al. (2020)	Hemp (Industrial bricks masonry wall)	In-plane	+ 286.57%	[86]
Mercedes et al. (2020)	Cotton (Industrial bricks masonry wall)	In-plane	+ 300.27%	[86]
Mercedes et al. (2020)	Glass (Industrial bricks masonry wall)	In-plane	+ 266.44%	[86]
Ponte et al. (2023)	Glass (rubbel stone masonry wall)	In-plane	+ 14.95%	[87]
Ponte et al. (2023)	Carbon (rubbel stone masonry wall)	In-plane	+ 14.43%	[87]
Torres et al. (2021)	Glass (Industrial brick masonry wall)	In-plane	+ 141.64	[88]

+ is the increement (average) with respect to the un-strengthed (reference) masonry wall.

3.1.4. Collapses in-plane load tests

The collapse scenario for each wall presents a diagonal crack denoting the edge between a compressive and a tensile stress pattern. Indeed, in the wall specimen subjected to vertical and horizontal load in its plane at the ultimate limit state, there is the development of a strut and tie system. The strut is almost diagonal, connecting the upper side where the hydraulic jack is applying the force with the lower side where there is the boundary condition. The diagonal crack is visible in Fig. 25.

Fig. 26 (left) presents the internal skeleton of the masonry wall HBW5, which shows the various layers of the TRM system. The TRM system starts with a lower mortar layer, on which the net was placed for structural upgrade, thereafter the jute fiber composite upper layer was applied for the masonry wall thermal upgrade.

An interesting collapse has been observed for the masonry wall-HBW3 and it is reported in Fig. 26 (right side). In this case, the TRM matrix (textile and mortar) gets separated/detached from the substrate, i.e., Debonding at the matrix-to-substrate interface has been observed. It is also possible to note that the jute net helps in holding the TRM layer.

3.1.5. Discussion and some observed limitations

The comparative analysis in Table 11 indicates that the proposed jute fiber NFTRM system, which consists of jute nets, jute dilatons, and jute-based composite mortar, enhances the load-carrying capacity (about) of masonry walls. This improvement is significantly higher than that obtained in earlier studies.

To illustrate this, consider the improvement obtained with hemp, cotton, and glass fibers, which were applied to industrial brick masonry, yielding 286.57%, 300.27%, and 266.44% improvement, respectively. Furthermore, glass fibers, as presented by Torres et al., showed an improvement of 141.64%. When applied to rubble stone masonry, however, relatively lower improvement of about 15% was obtained for glass and carbon fibers. The effectiveness of a reinforcement system strongly depends on both the mechanical properties of the reinforcing material and the characteristics of the masonry substrate. The results of the present study indicate that the proposed jute-based NFTRM system represents a sustainable alternative to synthetic fiber solutions and is capable of significantly improving the load-carrying capacity of masonry walls.

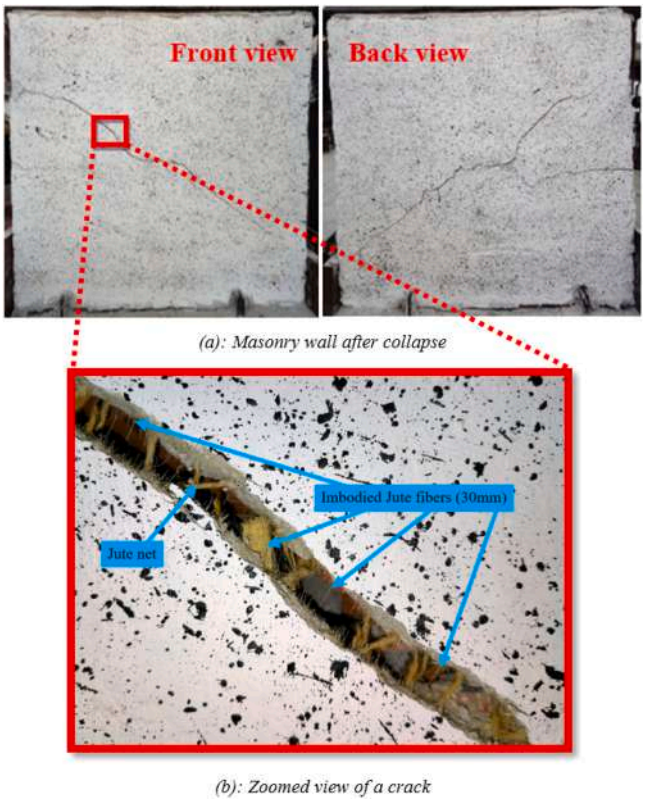

Fig. 25. Masonry wall-HBW5 after the collapse.

During the experimental campaign, some limits and practical difficulties were found, which must be highlighted when discussing the results. First of all, as far as natural fibers' properties are concerned, some material heterogeneity was found. In fact, even if a selection of jute fibers was made, some heterogeneity in terms of diameter, stiffness, and water absorption capacity was found, affecting the workability of the mortars and the homogeneity of the composite material. The control of fibers' moisture content was a practical difficulty, especially in terms of water content dosage.

Secondly, the process of making the jute net and diaton was a labor-intensive process. Although a slight irregularity in geometry may have been introduced in the manual preparation of the nets and their positioning, this may not have had a significant impact on uniform stress distribution. Similarly, drilling holes for diatons and their insertion into the transverse direction required precision to avoid damage to the bricks.

Thirdly, the attainment of a consistent bond between the NFTRM layers and the masonry substrate was also a key concern. As a matter of fact, in some specimens, a partial debonding phenomenon at the interface between the matrix and the substrate was observed at the ultimate stages of the test, which points to the sensitivity of the system under consideration.

Other problems encountered during the experiment were the slight asymmetries in the load-displacement relationships, which could be explained by the sensor position tolerance and the slight changes in the boundary conditions during the cyclic loading. Moreover, the stability of the vertical load during the cyclic test also had to be carefully monitored.

Finally, the campaign was limited to laboratory-scale masonry wall specimens under controlled conditions. Long-term durability aspects, environmental effects, and large-scale structural applications were beyond the scope of this study and require further investigation.

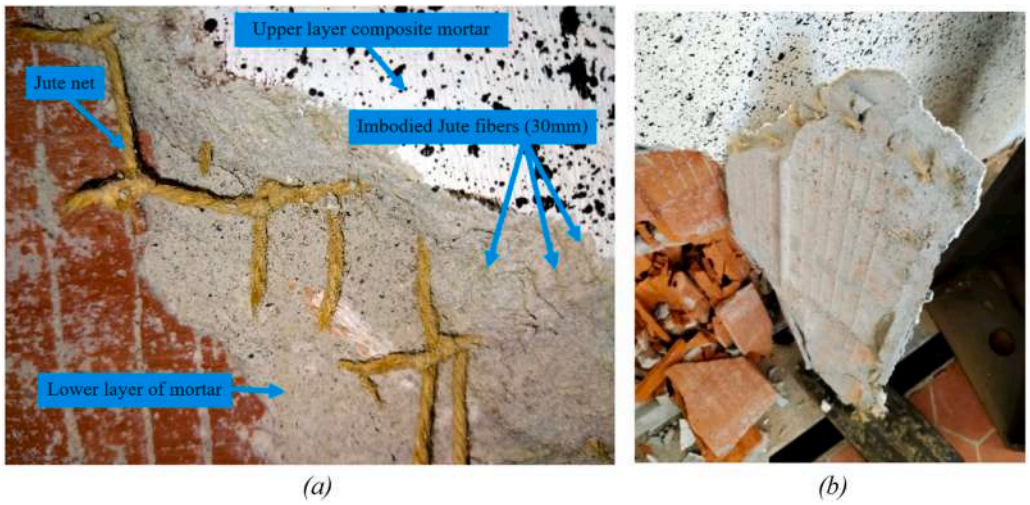

Fig. 26. (a) Composite structure (masonry wall-HBW5), and (b) Local collapse of a masonry structure (HBW3).

Despite these limitations, the experimental programme provided consistent and meaningful results, offering valuable insight into the structural behavior of jute-based NFTRM strengthening systems.

4. Conclusion

This study investigated a sustainable strengthening strategy for hollow brick masonry walls using a Natural Fiber Textile-Reinforced Mortar (NFTRM) system composed of jute fiber nets, jute diatons, and a jute-reinforced composite mortar layer. The experimental programme included in-plane cyclic shear tests under constant vertical loads, enabling a direct comparison between unstrengthened and strengthened specimens.

The results demonstrate that the NFTRM system provides a substantial enhancement in structural performance. The ultimate shear capacity of the strengthened walls increased by more than 455% compared with the reference specimens, while the calculated ultimate tensile strength of the NFTRM system remained consistently within 2.7–3.1 MPa across all configurations. These findings confirm the ability of jute-based reinforcements to deliver reliable mechanical behaviour despite the natural variability of the material.

The study also indicates that the addition of a jute-fiber composite mortar layer can slightly increase the ultimate capacity of the NFTRM system. However, further work is required to optimize key design parameters, including the number of textile layers, the equivalent thickness of the composite system, and the interaction between nets, diatons, and mortar. Additional testing—particularly under combined structural and thermal demands—will be essential to develop design-oriented models and facilitate the adoption of jute-based NFTRM systems in real construction practice.

The results support the viability of jute fiber NFTRM as a low-impact, renewable, and effective strengthening solution for masonry structures, especially in seismic-prone regions.

Notably, the research on NFTRM is very limited; therefore, this research contributes to enriching the knowledge and expanding the existing database on TRM (fully bio-based NFTRM) system. Further, it justifies the feasibility of the use of natural fibers (such as jute) as a reliable and significant structural enhancement. This innovative NFTRM retrofitting/upgrading system is conceptually comparable to conventional systems in terms of substantially lower environmental impact. This research will further encourage the integration of greener materials for various structural strengthening and structural performance evaluations. Therefore, based on the sustainability principles, this study provides a scientific basis for incorporating fiber composites into performance-oriented design frameworks.

CRediT authorship contribution statement

Mislav Stepinac: Writing – review & editing, Validation, Conceptualization. **Enzo Martinelli:** Writing – review & editing, Validation, Supervision, Conceptualization. **Monica Valdes:** Writing – review & editing, Methodology, Investigation, Data curation. **Arumugaprabu Veerasimman:** Writing – review & editing, Validation, Conceptualization. **Flavio Stochino:** Writing – review & editing, Writing – original draft, Validation, Supervision, Project administration, Investigation, Funding acquisition, Formal analysis, Conceptualization. **Arnas Majumder:** Writing – review & editing, Writing – original draft, Methodology, Investigation, Data curation, Conceptualization.

Funding

The authors gratefully acknowledge the financial support provided by the PRIN PNRR 2022 project Integra TRM: Integrated Seismic and Thermal Upgrading of Existing Masonry Buildings through a Novel Sustainable Textile-Reinforced Mortar System (F53D23009850001), as well as by the RELUIS–DPC 2024–2026 Project, Work Package 5.

Declaration of Competing Interest

The authors declare that they have no known competing financial interests or personal relationships that could have appeared to influence the work reported in this paper.

References

[1] Acito M, Magrinelli E, Milani G, Tiberti S. Seismic vulnerability of masonry buildings: numerical insight on damage causes for residential buildings by the 2016 central Italy seismic sequence and evaluation of strengthening techniques. J Build Eng 2020;28:101081. https://doi.org/10.1016/j.jobe.2019.101081.
[2] Di Chicco R, Chieffo N, Formisano A. Exposure and seismic vulnerability of masonry buildings grouped in aggregate of a typical historical centre in the Basilicata region of Italy. J Build Eng 2024;94:109859. https://doi.org/10.1016/j.jobe.2024.109859.
[3] Amitrano L, Di Chicco R, Formisano A. Seismic vulnerability and fragility assessment of masonry structures within the historic centre of Meta (Naples, Southern Italy). J Build Eng 2025;104:112328. https://doi.org/10.1016/j.jobe.2025.112328.
[4] Türkmen ÖS, Vries BTD, Wijte SNM, Ingham JM. Out-of-plane behaviour of clay brick masonry walls retrofitted with flexible deep mounted CFRP strips and additional single-sided FRCM overlay. Structures 2021;33:2459–74. https://doi.org/10.1016/j.istruc.2021.05.061.
[5] Hadi S, Kazeminezhad E, Safakhah S. Full-scale experimental evaluation of flexural strength and ductility of reinforced concrete beams strengthened with various FRP mechanisms. Structures 2022;43:1160–76. https://doi.org/10.1016/j.istruc.2022.07.011.

[6] Konthesingha KMC, Masia MJ, Petersen RB, Mojsilovic N, Simundic G, Page AW. Static cyclic in-plane shear response of damaged masonry walls retrofitted with NSM FRP strips – An experimental evaluation. Eng Struct 2013;50:126–36. https://doi.org/10.1016/j.engstruct.2012.10.026.

[7] Mostofinejad D, Hajrasouliha M. 3D beam–column corner joints retrofitted with X-shaped FRP sheets attached via the EBROG technique. Eng Struct 2019;183:987–98. https://doi.org/10.1016/j.engstruct.2019.01.038.

[8] Wu C, Ma G, Hwang H-J. Bond performance of spliced GFRP bars in pre-damaged concrete beams retrofitted with CFRP and UHPC. Eng Struct 2023;292:116523. https://doi.org/10.1016/j.engstruct.2023.116523.

[9] Soleymani A, Najafgholipour MA, Johari A, Dooshabi A. The diagonal shear behavior of masonry walls fabricated with historical lime-based mortar and retrofitted with near surface mounted method. Structures 2024;59:105795. https://doi.org/10.1016/j.istruc.2023.105795.

[10] Abdulsalam B, Ali AH, ElSafty A, Elshafey N. Behavior of GFRP strengthening masonry walls using glass fiber composite anchors. Structures 2021;29:1352–61. https://doi.org/10.1016/j.istruc.2020.12.025.

[11] Alecci V, Barducci S, D'Ambrisi A, De Stefano M, Focacci F, Luciano R, Penna R. Shear capacity of masonry panels repaired with composite materials: Experimental and analytical investigations. Composites Part B Engineering 2019;171:61–9. https://doi.org/10.1016/j.compositesb.2019.04.013.

[12] Reichenbach S, Preinstorfer P, Hammerl M, Kromoser B. A review on embedded fibre-reinforced polymer reinforcement in structural concrete in Europe. Constr Build Mater 2021;307:124946. https://doi.org/10.1016/j.conbuildmat.2021.124946.

[13] L.A. Bisby, B.K. Williams, M.F. Green, V.K.R. Kodur, STUDIES ON THE FIRE BEHAVIOUR OF FRP REINFORCED AND/OR STRENGTHENED CONCRETE MEMBERS, (n.d.).

[14] Askouni PD, Polydoropoulos S, Papanicolaou CG. Textile Reinforced Mortar/masonry joints under reverse cyclic in-plane shear. Constr Build Mater 2023;403:133122. https://doi.org/10.1016/j.conbuildmat.2023.133122.

[15] Ameli Z, D'Antino T, Carloni C. A new predictive model for FRCM-confined columns: A reflection on the composite behavior at peak stress. Constr Build Mater 2022;337:127534. https://doi.org/10.1016/j.conbuildmat.2022.127534.

[16] Jing L, Wang N, Yin S. Shear performance of textile-reinforced concrete (TRC)-strengthened brick masonry walls. Constr Build Mater 2023;397:132401. https://doi.org/10.1016/j.conbuildmat.2023.132401.

[17] Angiolilli M, Gregori A, Cattari S. Performance of Fiber Reinforced Mortar coating for irregular stone masonry: Experimental and analytical investigations. Constr Build Mater 2021;294:123508. https://doi.org/10.1016/j.conbuildmat.2021.123508.

[18] CNR-DT 2018. CNR-DT, Guide for the design and construction of externally bonded fibre reinforced inorganic matrix systems for strengthening existing structures, (2018).

[19] Ferrara G. Flax-TRM Composite Systems for Strengthening of Masonry: F. rom Material Identification to Structural Behavior. Cham: Springer International Publishing; 2021. https://doi.org/10.1007/978-3-030-70273-1.

[20] Torunbalcı N, Onar E, Günay H. Structural evaluation of masonry walls with double-sided CFRP reinforcement through diagonal compression tests. J Build Eng 2025;111:113142. https://doi.org/10.1016/j.jobe.2025.113142.

[21] Faella C, Martinelli E, Nigro E, Paciello S. Shear capacity of masonry walls externally strengthened by a cement-based composite material: An experimental campaign. Constr Build Mater 2010;24:84–93. https://doi.org/10.1016/j.conbuildmat.2009.08.019.

[22] Prota A, Marcari G, Fabbrocino G, Manfredi G, Aldea C. Experimental in-plane behavior of tuff masonry strengthened with cementitious matrix–grid composites. J Compos Constr 2006;10:223–33. https://doi.org/10.1061/(ASCE)1090-0268(2006)10:3(223).

[23] Akhoundi F, Vasconcelos G, Lourenço P. In-Plane Behavior of Infills using Glass Fiber Shear Connectors in Textile Reinforced Mortar (TRM) Technique. Int J Struct Glass Adv Mater Res 2018;2:1–14. https://doi.org/10.3844/sgamrsp.2018.1.14.

[24] Bernat E, Gil L, Roca P, Escrig C. Experimental and analytical study of TRM strengthened brickwork walls under eccentric compressive loading. Constr Build Mater 2013;44:35–47. https://doi.org/10.1016/j.conbuildmat.2013.03.006.

[25] Ferrara G, Caggegi C, Gabor A, Martinelli E. Experimental Study on the Adhesion of Basalt Textile Reinforced Mortars (TRM) to Clay Brick Masonry: The Influence of Textile Density. Fibers 2019;7:103. https://doi.org/10.3390/fib7120103.

[26] Fossetti M, Minafò G. Strengthening of Masonry Columns with BFRCM or with Steel Wires: An Experimental Study. Fibers 2016;4:15. https://doi.org/10.3390/fib4020015.

[27] Piazzon R, Niero L, Zampieri P, Pellegrino C. Effects on the shear behaviour of existing masonry walls strengthened with one-sided SFRM coating. J Build Eng 2025;111:113373. https://doi.org/10.1016/j.jobe.2025.113373.

[28] Gong J, Ma Y, Fu J, Hu J, Ouyang X, Zhang Z, Wang H. Utilization of fibers in ultra-high performance concrete: A review. Compos Part B Eng 2022;241:109995. https://doi.org/10.1016/j.compositesb.2022.109995.

[29] Revanna N, Moy CKS. Experimental study on reinforced concrete beams strengthened with Basalt and Carbon Textile Reinforced mortars at elevated temperatures. Eng Struct 2024;307:117921. https://doi.org/10.1016/j.engstruct.2024.117921.

[30] Mercimek Ö, Çelik A, Ghoroubi R, Anil Ö. Retrofitting of squat RC column by using TRM strip under axial load. Structures 2024;60:105909. https://doi.org/10.1016/j.istruc.2024.105909.

[31] Guo L, Deng M, Li T. Seismic behaviour of RC columns retrofitted with textile-reinforced mortar (TRM) optimized by short PVA fibres. Structures 2023;50:244–54. https://doi.org/10.1016/j.istruc.2023.02.041.

[32] Ramezani A, Esfahani MR. Shear strengthening of RC beams using FRCM system made with industrial wastes. Structures 2023;48:1833–47. https://doi.org/10.1016/j.istruc.2023.01.078.

[33] Campolongo F, Cascardi A, Ombres L. Prediction of the additional compressive strength due to PBO-FRCM-confinement of brick-masonry depending on the stiffening effect caused by different discontinuous wrappings: new design-oriented perspective. Structures 2023;57:105124. https://doi.org/10.1016/j.istruc.2023.105124.

[34] Bertolesi E, Torres B, Adam JM, Calderón PA, Moragues JJ. Effectiveness of Textile Reinforced Mortar (TRM) materials for the repair of full-scale timbrel masonry cross vaults. Eng Struct 2020;220:110978. https://doi.org/10.1016/j.engstruct.2020.110978.

[35] Dong Z, Deng M, Dai J, Ma P. Diagonal compressive behavior of unreinforced masonry walls strengthened with textile reinforced mortar added with short PVA fibers. Eng Struct 2021;246:113034. https://doi.org/10.1016/j.engstruct.2021.113034.

[36] Ivorra S, Torres B, Baeza FJ, Bru D. In-plane shear cyclic behavior of windowed masonry walls reinforced with textile reinforced mortars. Eng Struct 2021;226:111343. https://doi.org/10.1016/j.engstruct.2020.111343.

[37] Furtado A, Rodrigues H, Arêde A, Varum H. Impact of the Textile Mesh on the Efficiency of TRM Strengthening Solutions to Improve the Infill Walls Out-of-Plane Behaviour. Appl Sci 2020;10:8745. https://doi.org/10.3390/app10238745.

[38] Mezrea PE, Ispir M, Balci IA, Bal IE, Ilki A. Diagonal tensile tests on historical brick masonry wallets strengthened with fabric reinforced cementitious mortar. Structures 2021;33:935–46. https://doi.org/10.1016/j.istruc.2021.04.076.

[39] Furtado A, Rodrigues H, Arêde A, Varum H. A experimental characterization of seismic plus thermal energy retrofitting techniques for masonry infill walls. J Build Eng 2023;75:106854. https://doi.org/10.1016/j.jobe.2023.106854.

[40] Karlos K, Tsantilis A, Triantafillou T. Integrated Seismic and Energy Retrofitting System for Masonry Walls Using Textile-Reinforced Mortars Combined with Thermal Insulation: Experimental, Analytical, and Numerical Study. J Compos Sci 2020;4:189. https://doi.org/10.3390/jcs4040189.

[41] Gkournelos PD, Triantafillou TC, Bournas DA. Integrated Structural and Energy Retrofitting of Masonry Walls: Effect of In-Plane Damage on the Out-of-Plane Response. J Compos Constr 2020;24:04020049. https://doi.org/10.1061/(ASCE)CC.1943-5614.0001066.

[42] Triantafillou TC, Karlos K, Kefalou K, Argyropoulou E. An innovative structural and energy retrofitting system for URM walls using textile reinforced mortars combined with thermal insulation: Mechanical and fire behavior. Constr Build Mater 2017;133:1–13. https://doi.org/10.1016/j.conbuildmat.2016.12.032.

[43] Triantafillou TC, Karlos K, Kapsalis P, Georgiou L. Innovative Structural and Energy Retrofitting System for Masonry Walls Using Textile Reinforced Mortars Combined with Thermal Insulation: In-Plane Mechanical Behavior. J Compos Constr 2018;22:04018029. https://doi.org/10.1061/(ASCE)CC.1943-5614.0000869.

[44] Gkournelos PD, Triantafillou TC. Out-of-Plane Behavior of In-Plane Damaged Masonry Infills Retrofitted with TRM and Thermal Insulation. J Compos Constr 2023;27:04023054. https://doi.org/10.1061/JCCOF2.CCENG-4324.

[45] Vu VT, Lai DY. Approaches to characterizing human health risks of exposure to fibers. Environ Health Perspect 1997;105:1329–36. https://doi.org/10.1289/ehp.97105s51329.

[46] EC, Construction and demolition waste, European Commission, Brussels, Belgium, n.d. ⟨https://environment.ec.europa.eu/topics/waste-and-recycling/construction-and-demolition-waste_en⟩ (accessed April 20, 2024).

[47] Majumder A, Stochino F, Frattolillo A, Valdes M, Gatto G, Martinelli E. Sustainable Retrofitting Solutions: Evaluating the Performance of Jute Fiber Nets and Composite Mortar in Natural Fiber Textile Reinforced Mortars. Sustainability 2024;16:1175. https://doi.org/10.3390/su16031175.

[48] EU Directive 2008/98/EC, Directive 2008/98/EC of the European Parliament and of the Council of 19 November 2008 on Waste and Repealing Certain Directives., (2008). ⟨http://Data.Europa.Eu/Eli/Dir/2008/98/2018-07-05⟩ (accessed April 20, 2024).

[49] de Beus N, Carus M, Barth M. Natural Fibres Show Outstandingly Low CO2 Footprint Compared to Glass and Mineral Fibres – Nova-Institute Updates its Reference Study for the Automotive and Insulation Industry. PRESS RELEASE; 2019. ⟨https://renewable-carbon.eu/news/natural-fibres-show-outstandingly-low-co2-footprint-compared-to-glass-and-mineral-fibres/⟩ (accessed December 12, 2023).

[50] Majumder A, Stochino F, Fraternali F, Martinelli E. Seismic and Thermal Retrofitting of Masonry Buildings with Fiber Reinforced Composite Systems: A State of the Art Review. Int J Struct Glass Adv Mater Res 2021;5:41–67. https://doi.org/10.3844/sgamrsp.2021.41.67.

[51] Valenza A, Fiore V, Nicolosi A, Rizzo G, Scaccianoce G, Bella GDi. Effect of sheep wool fibres on thermal-insulation and mechanical properties of cement matrix. Acad J Civ Eng 2015:40–5. https://doi.org/10.26168/ICBBM2015.5.

[52] Benmansour N, Agoudjil B, Gherabli A, Kareche A, Boudenne A. Thermal and mechanical performance of natural mortar reinforced with date palm fibers for use as insulating materials in building. Energy Build 2014;81:98–104. https://doi.org/10.1016/j.enbuild.2014.05.032.

[53] Raut AN, Gomez CP. Thermal and mechanical performance of oil palm fiber reinforced mortar utilizing palm oil fly ash as a complementary binder. Constr Build Mater 2016;126:476–83. https://doi.org/10.1016/j.conbuildmat.2016.09.034.

[54] Vailati M, Mercuri M, Angiolilli M, Gregori A. Natural-Fibrous Lime-Based Mortar for the Rapid Retrofitting of Heritage Masonry Buildings. Fibers 2021;9:68. https://doi.org/10.3390/fib9110068.

[55] Santos GZBD, Caldas LR, Melo Filho JDA, Monteiro NBR, Rafael SIM, Marques Da Silva N. Circular alternatives in the construction industry: An environmental performance assessment of sisal fiber-reinforced composites. J Build Eng 2022;54:104603. https://doi.org/10.1016/j.jobe.2022.104603.
[56] Tang L, Liu T, Sun P, Wang Y, Liu G. Sisal fiber modified construction waste recycled brick as building material: Properties, performance and applications. Structures 2022;46:927–35. https://doi.org/10.1016/j.istruc.2022.10.126.
[57] Codispoti R, Oliveira DV, Olivito RS, Lourenço PB, Fangueiro R. Mechanical performance of natural fiber-reinforced composites for the strengthening of masonry. Compos Part B Eng 2015;77:74–83. https://doi.org/10.1016/j.compositesb.2015.03.021.
[58] Hari R, Mini KM. Mechanical and durability properties of sisal-Nylon 6 hybrid fibre reinforced high strength SCC. Constr Build Mater 2019;204:479–91. https://doi.org/10.1016/j.conbuildmat.2019.01.217.
[59] Elfordy S, Lucas F, Tancret F, Scudeller Y, Goudet L. Mechanical and thermal properties of lime and hemp concrete ("hempcrete") manufactured by a projection process. Constr Build Mater 2008;22:2116–23. https://doi.org/10.1016/j.conbuildmat.2007.07.016.
[60] Filazi A, Tortuk S, Pul M. Determination of optimum blast furnace slag ash and hemp fiber ratio in cement mortars. Structures 2023;57:105024. https://doi.org/10.1016/j.istruc.2023.105024.
[61] Rahimi M, Hisseine OA, Tagnit-Hamou A. Effectiveness of treated flax fibers in improving the early age behavior of high-performance concrete. J Build Eng 2022;45:103448. https://doi.org/10.1016/j.jobe.2021.103448.
[62] Yan Z-W, Bai Y-L, Zhang Q, Zeng J-J. Experimental study on dynamic properties of flax fiber reinforced recycled aggregate concrete. J Build Eng 2023;80:108135. https://doi.org/10.1016/j.jobe.2023.108135.
[63] Zhao H, Li Z, Tang J, Zhou T, Xiong T, Gao X. Reducing steel fiber segregation and enhancing UHPC performance with hybrid bamboo fibers: An eco-friendly approach. J Build Eng 2025;107:112741. https://doi.org/10.1016/j.jobe.2025.112741.
[64] Shi J, Lu Y, Zhu R, Liu Y, Zhang Y, Lv Q. Experimental evaluation of fracture toughness of bamboo fiber reinforced high performance lightweight aggregate concrete. Eng Struct 2023;297:117028. https://doi.org/10.1016/j.engstruct.2023.117028.
[65] Ferrara G, Pepe M, Toledo Filho RD, Martinelli E. Mechanical Response and Analysis of Cracking Process in Hybrid TRM Composites with Flax Textile and Curauá Fibres. Polymers 2021;13:715. https://doi.org/10.3390/polym13050715.
[66] Teixeira FP, Cardoso DCT, De Andrade Silva F. On the shear behavior of natural curauá fabric reinforced cement-based composite systems. Eng Struct 2021;246:113054. https://doi.org/10.1016/j.engstruct.2021.113054.
[67] Alam MdA, Al Riyami K, Bakkar S. Optimization of kenaf fibre reinforced polymer laminate for shear strengthening of RC beams using embedded connector. Eng Struct 2021;232:111790. https://doi.org/10.1016/j.engstruct.2020.111790.
[68] Helaili S, Chafra M, Chevalier Y. Natural fiber alfa/epoxy randomly reinforced composite mechanical properties identification. Structures 2021;34:542–9. https://doi.org/10.1016/j.istruc.2021.07.095.
[69] Meglio E, Formisano A. Hemp-based systems as seismic strenghtening interventions of existing masonry buildings. J Build Eng 2025;112:113786. https://doi.org/10.1016/j.jobe.2025.113786.
[70] Trochoutsou N, Di Benedetti M, Pilakoutas K, Guadagnini M. Mechanical Characterisation of Flax and Jute Textile-Reinforced Mortars. Constr Build Mater 2021;271:121564. https://doi.org/10.1016/j.conbuildmat.2020.121564.
[71] Khaleel S, Madhavi K, Basutkar SM. Mechanical characteristics of brick masonry using natural fiber composites. Mater Today Proc 2021;46:4817–24. https://doi.org/10.1016/j.matpr.2020.10.319.
[72] Pepe M, Lombardi R, Ferrara G, Agnetti S, Martinelli E. Experimental Characterisation of Lime-Based Textile-Reinforced Mortar Systems Made of Either Jute or Flax Fabrics. Materials 2023;16:709. https://doi.org/10.3390/ma16020709.
[73] Menna C, Asprone D, Durante M, Zinno A, Balsamo A, Prota A. Structural behaviour of masonry panels strengthened with an innovative hemp fibre composite grid. Constr Build Mater 2015;100:111–21. https://doi.org/10.1016/j.conbuildmat.2015.09.051.
[74] Ferrara G, Caggegi C, Martinelli E, Gabor A. Shear capacity of masonry walls externally strengthened using Flax-TRM composite systems: experimental tests and comparative assessment. Constr Build Mater 2020;261:120490. https://doi.org/10.1016/j.conbuildmat.2020.120490.
[75] UN, Future fibers, Jute., Food and agriculture organization of the United Nations, n.d. ⟨https://www.fao.org/economic/futurefibres/fibres/jute/en/⟩ (accessed April 25, 2024).
[76] T. Townsend, Natural Fibres and the World Economy July 2019, (n.d.). ⟨https://dnfi.org/natural-fibres-and-the-world-economy-july-2019⟩ (accessed December 12, 2023).
[77] Islam MdS, Ahmed SK. The Impacts of Jute on. Environ Anal Rev Bangladesh 2012;2. ⟨https://www.iiste.org/Journals/index.php/JEES/article/viewFile/1999/1978⟩.
[78] Bambach MR. Direct Comparison of the Structural Compression Characteristics of Natural and Synthetic Fiber-Epoxy Composites: Flax, Jute, Hemp, Glass and Carbon Fibers. Fibers 2020;8:62. https://doi.org/10.3390/fib8100062.
[79] Majumder A, Stochino F, Frattolillo A, Valdes M, Mancusi G, Martinelli E. Jute fiber-reinforced mortars: mechanical response and thermal performance. J Build Eng 2023;66:105888. https://doi.org/10.1016/j.jobe.2023.105888.
[80] Majumder A, Stochino F, Farina I, Valdes M, Fraternali F, Martinelli E. Physical and mechanical characteristics of raw jute fibers, threads and diatons. Constr Build Mater 2022;326:126903. https://doi.org/10.1016/j.conbuildmat.2022.126903.
[81] NTC18, NTC18 Italian building code 'Norme Tecniche per le Costruzioni ' Ministero delle infrastrutture e dei Trasporti, in Italian., (n.d.)..
[82] NTC18, NTC18 Application Circular of NTC18 (2019). Circolare n. 7 del 21 Gennaio 2019,"Istruzioni per l'applicazione dell'«Aggiornamento delle "Norme tecniche per le costruzioni"» in Italian., (n.d.).
[83] CEN, Methods of test for mortar for masonry – Part 11: Determination of flexural and compressive strength of hardened mortar, (2019).
[84] EN 13501-1, Fire Classification of Products and Building Elements - Part1: Classification Using Data from Reaction to Fire Tests., (2019).
[85] Poroton Italia, Blocchi semipieni P800, (n.d.). ⟨https://www.poroton.it/mattoni-laterizi/blocchi-semipieni-p800/⟩ (accessed March 4, 2024).
[86] Mercedes L, Bernat-Maso E, Gil L. In-plane cyclic loading of masonry walls strengthened by vegetal-fabric-reinforced cementitious matrix (FRCM) composites. Eng Struct 2020;221:111097. https://doi.org/10.1016/j.engstruct.2020.111097.
[87] Ponte M, Penna A, Bento R. In-plane cyclic tests of strengthened rubble stone masonry. Mater Struct 2023;56:41. https://doi.org/10.1617/s11527-023-02126-8.
[88] Torres B, Ivorra S, Javier Baeza F, Estevan L, Varona B. Textile reinforced mortars (TRM) for repairing and retrofitting masonry walls subjected to in-plane cyclic loads. An experimental approach. Eng Struct 2021;231:111742. https://doi.org/10.1016/j.engstruct.2020.111742.